INVESTIGATION OF FLOW THROUGH A SEMI AXIAL CENTRIFUGAL PUMP

A Thesis Submitted to
The Graduate School of Engineering and Sciences of
İzmir Institute of Technology
In Partial Fulfillment of the Requirements for the Degree of

MASTER OF SCIENCE

in Mechanical Engineering

by
Yılmaz KARAMANOĞLU

July 2006
İZMİR

We approve the thesis of **Yılmaz KARAMANOĞLU**

Date of Signature

……. **13 July 2006**
Asst. Prof. Dr. Moghtada MOBEDI
Supervisor
Department of Mechanical Engineering
İzmir Institute of Technology

……. **13 July 2006**
Prof. Dr. Zafer İLKEN
Department of Mechanical Engineering
İzmir Institute of Technology

……. **13 July 2006**
Asst. Prof. Dr. Aytunç EREK
Department of Mechanical Engineering
Dokuz Eylül University

……. **13 July 2006**
Assoc. Prof. Dr. Barış ÖZERDEM
Department of Mechanical Engineering
Head of Department
İzmir Institute of Technology

…….
Assoc. Prof. Dr. Semahat ÖZDEMİR
Head of Graduate School

ACKNOWLEDGMENTS

I would like to express my great appreciation to A. Özden Ertöz for all his support during my graduate education. He has guided me with his great patience and tolerance. Also I should like to express my deepest gratitude to Tunç Değer and Ender Duymuş, and all other VANSAN stuff for their great guidance, support and contribution to me.

I should definitely express my gratitude to Prof. Dr. Macit Toksoy. From my undergraduate, he supported me too much and motivate for graduation. Also he provides many opportunities

Special and very sincere thanks to my advisor Asst. Prof. Dr. Moghtada Mobedi for his great patience and support. During the day we met, his great knowledge and diligence motivates me to work harder.

Thanks to M. Özer Gelişli, the technical manager of the ANOVA. He answered all my questions with his great knowledge about CFD.

Finally, for their great support and patience during whole my education, I should express my love to my parents, and my sister Aynur.

ABSTRACT

INVESTIGATION OF FLOW THROUGH A SEMI AXIAL CENTRIFUGAL PUMP

The aim of present study is to perform a numerical work to investigate flow inside a semi axial centrifugal pump. The results of the study can be used to improve the design of the pump.

The Navier Stokes equations with appropriate boundary conditions are solved for a 3 dimensional rotating geometry. To solve the governing equations, Fluent program is used. Fluent is a commercial CFD program, which has been developed based on the finite volume method. The mesh for the flow volume is created by Gambit. The $k-\varepsilon$ turbulence model is used to handle the turbulence inside the flow. Obtained results are compared with experimental test results. An acceptable agreement between the numerical and experimental results is observed.

Based on the obtained results, the velocity vectors, pressure distributions on impeller and diffuser blades and flow patterns are plotted for three different flow rates. The necessary discussions are performed for these results. It is observed that the design of the impeller provides a regular flow inside the channel; however some vortexes are observed in the channel between the diffuser blades.

The effect of the surface roughness is also investigated and the problem is solved for four different roughness values (0, 50, 100 and 250 μm). It is found that the roughness of the surface affects the characteristic curves of the pump. By increasing the roughness, the head and efficiency of the pump decrease however the consumed power is almost constant.

ÖZET

YARI EKSENEL SANTRİFUJ BİR POMPANIN İÇİNDEKİ AKIŞIN İNCELENMESİ

Bu çalışmanın amacı, yarı eksenel santrifüj bir pompa içindeki akışı incelemek için nümerik bir çalışma gerçekleştirmektir. Bu çalışmanın sonuçları bir pompa tasarımının geliştirilmesinde kullanılabilinir.

Navier Stokes denklemleri, uygun sınır koşulları ile 3 boyutlu döner bir geometri için çözülmüştür. Probleme ait denklemler Fluent programı ile çözülmüştür. Fluent, sonlu hacimler tekniği üzerine geliştirilmiş ticari bir HAD programıdır. Akış hacmi için oluşturulan sayısal ağ ise Gambit programında oluşturulmuştur. Akışın içindeki türbülans için $k-\varepsilon$ türbülans modeli kullanılmıştır. Elde edilen sonuçlar, hassas test sonuçları ile karşılaştırılmıştır. Nümerik ve deneysel sonuçlar arasında kabul edilebilir bir uyuşma gözlemlenmiştir.

Elde edilen sonuçlara dayanarak, 3 farklı debi için hız vektörleri, çarktaki ve difizördeki basınç dağılımları ve akış yörüngeleri çizdirilmiştir. Bu sonuçlar için gerekli olan görüşler belirtilmiştir. Çarkın dizaynının, çarkın kanatları arasındaki kanaldaki akışın düzgün olmasını sağladığı görülmüştür. Fakat difizör kanatları arasındaki akışta burulmalar gözlemlenmiştir.

Yüzey pürüzlülüğün etkisi de ayrıca incelenmiş, ve problem 4 farklı yüzey pürüzlülük değeri (0, 50, 100 and 250 μm) için çözülmüştür. Yüzey pürüzlüğünün pompanın karakteristik eğrilerine etkidiği gözlemlenmiştir.Yüzey pürüzlülüğünü arttırarak, pompanın basma yüksekliği düşmüş, fakat pompanın çektiği güç hemen hemen aynı kalmıştır.

TABLE OF CONTENTS

LIST OF FIGURES

LIST OF TABLES

LIST OF SYMBOLS

H	Head	mWC
g	Gravitational constant	m/s^2
Q	Mass flow rate	kg/s
n	Rotational speed	rpm
n_ω	Specific speed	$nQ^{1/2}/(gH)^{3/4}$
$\vec{V}$	Velocity vector	m/s
p_0	Total pressure	Pa
p_s	Static pressure	Pa
p_d	Dynamic pressure	Pa
P	Power	W
F_{BODY}	Body forces (external forces)	N
h	Total enthalpy	kJ/kg
T	Torque	$N-m$
T	Temperature	C
k	Thermal conductivity	$W/m-K$
k	Turbulence kinetic energy	J
M	Mach number	
Re	Reynolds number	
L	Characteristic length	m
P_k	Turbulence kinetic energy generation due to mean velocity	J
G_b	Turbulence kinetic energy generation due to buoyancy	J
u_r	Relative velocity	rad/s
$\vec{r}$	Position vector	

Ω	Angular velocity	m/s
η	Efficiency	$\%$
τ	Stress	Pa
ε	Turbulence dissipation rate	m^2/s^3
α	Isothermal compressibility	
β	Bulk expansion coefficient	K^{-1}
ν	Kinematic viscosity	m^2/s
μ	Dynamic viscosity	$Pa-s$
μ_t	Turbulence viscosity	$Pa-s$
ρ	Density	kg/m^3

CHAPTER 1

INTRODUCTION

Lots of machinery has been developed in order to transfer liquids, especially water, to higher locations, or forcing it against a resistance. These machines that add energy to a fluid stream are called pumps (Değer, 2005). Thus, as the water, pumps are also very important in daily life. From ancient times to now, they have vital roles in irrigation, fire extinguishing, industry, and water network systems. Among pump types, the centrifugal pumps are those that can suit any working condition, process with high efficiencies and the most widely used ones (van Esch, 1997).

Due to the work done, a pump consumes huge amounts of energy, which means high operating costs. According to a research made in Europe, the initial cost of a pump that operates about 20 years, constitutes just 5% of its lifecycle cost. However, 80% of rest is the operating cost and 15% is the maintenance cost respectively (Frenning, 2001). These lead the manufacturers to design and produce pumps with higher efficiencies in order to decrease the operating costs.

Pump designs are made by using empirical relations that have been developed based on the experiences. The first designs were made after the theoretical work of Euler in 1750. That study made the working principle of a pump a little clear. However, centrifugal pump design shows a great development after the “The Great Exhibition” (van Esch, 1997).

In the most of the pump factories, a preliminary design is performed in order to develop a pump. After the design is completed, the manufacturing models are processed, so that a prototype can be manufactured. Then this prototype pump is tested for verification of the design values. If the pump can not prove its design criteria, all the procedure is restarted until the obtained experimental results will satisfy the design criteria. This method of manufacturing is expensive and requires long design period.

Developments in the computer technology in the recent years, in both software and hardware, enable the pump design by using computers. The designers not only can design the required pump, but also can simulate fluid flow inside the pump. The development of the three-dimensional drawing softwares (computer aided design-

CAD), also causes development of the analysis software. Nowadays many mechanic, magnetic, fluid and noise problems can be numerically solved.

Computational fluid dynamics softwares are widely used in the industry and universities. Many commercial CFD programs have been developed to solve the governing equations of the fluid problem. Although the use of these softwares seems easy, user must have advanced knowledge of fluid dynamics and also numerical methods in order to set the appropriate boundary conditions and interpret the results. The accuracy of the results depends on the experience of the analyst. If the flow and parameters are properly defined, the obtained results will have high accuracy and reliability.

As mentioned before the traditional design procedure of a pump is complicated and expensive. The accuracy and performance of the design mostly depend on the experience of the designer. The efficiency of a pump at the operating conditions is an important parameter for a designer. The improvement of efficiency requires a great research and development work. The computational fluid dynamics softwares enable the designer to visualize both flow and pressure distributions inside the pump and minimize the experiment and verification costs. It also decreases the design period. However, the results of the computational analysis should match with experimental results.

The purpose of this study is to investigate the flow in the impeller and diffuser of a semi axial pump by using Computational Fluid Dynamics. For this reason, a semi axial pump of VANSAN Company is selected. The analyzed pump is a 14" vertical single stage turbine pump that consists of a 6 blades rotating impeller and a static diffuser with 7 blades. This pump is the one that was designed and researched by Duymuş (Duymuş, 2003). In Duymuş study, the pump was tested by sensitive test equipments and then the characteristic curves of the pump were obtained. In the present study, the problem is solved by the Fluent program. It is a commercial program which has been developed based on primitive variable approach in order to solve continuity, momentum, energy and mass transfer equations not only for laminar but also for turbulent flows. The program uses finite volume method to solve the governing equations.

The considered pump is firstly modeled and the three dimensional fluid model is constructed by the UniGraphics NX3 program. Then, the model is exported to the Gambit program for mesh generation. Then, the constructed mesh is exported to the main analysis program; Fluent. The boundary conditions are defined and the solution

methods are chosen. The $k-\varepsilon$ turbulence model is used to handle the turbulence of the flow. An acceptable agreement between the numerical and experimental study is observed. The flow inside the pump is investigated for seven different flow rates (from 90 kg/s to 150 kg/s with 10 kg/s interval). All the details about the employed solution procedure and the parameters are given in different chapters of this thesis. The static, dynamic and total pressure on the surfaces of impeller and diffuser are also studied. The pressure and velocity fields are plotted and necessary discussions are performed. Based on the obtained results, it is observed that the pressure distribution on the surfaces of the impeller blades and flow distribution inside the rotor are close to the desired distribution and values. However, in the diffuser, some vortexes occur and flow patterns are too far from the desired conditions. The pressure distribution on the blades of the diffuser is also far from the ideal and desired distribution.

The affect of the surface roughness on the characteristic of the pump is also handled. The roughness of the wall boundaries has a considerable affect on the pump characteristic curves. The head and efficiency of pump decreases by increase of the roughness, however, the required power is almost same.

1.1. Literature Survey

Numerical methods for solving differential equations were built in earlier times. However, since the computations are lasts long, and not accurate enough, there have not been obtained any significant success. With the invention of transistor, thus the computers, these calculations can be made in shorter periods. As the processors are developed more, finer and more accurate results are became available. Less assumptions and simplifications in the governing equations and more detailed definitions of the geometry by two dimensional or even there dimensional analysis, with possible unsteady conditions make the obtained results more realistic and valuable. Since the development of CFD is highly dependent to the development in the computer technology, the main studies and researches have been mainly done in the recent years.

Even there are many published studies in the literature, about the use of CFD within the turbomachinery concept; a few of them are about the semi axial centrifugal deep well pumps.

The closest work to this study is done by Bartholomeus Petrus Maria van Esch (van Esch, 1997). He showed that the flow in radial and mixed flow type pumps can be modeled with unsteady flow while considering the flow is incompressible potential flow. The effect of viscosity is modeled in the thin boundary layers, wakes and mixing areas. In his thesis, in order to solve the unsteady potential flow, he used fully three dimensional finite element methods. He divided the computational mesh into rotor and stator parts, and connected them with sliding interfaces. To reduce the computational time, he employed special numerical techniques based on subtracting method combined with the implicit imposition of the Kutta conditions at the trailing edges of the impeller and diffuser blades. His computational results showed a good agreement with the experimentally obtained values.

There also similar works done in Türkiye. One of them belongs to Ebru Suna Ergün (Ergün, 1999). She used a two dimensional impeller with 8 blades and a two dimensional diffuser and discretize them by finite element method. The flow has been modeled by the vorticity stream approach. Since the results are based on vorticity and streamlines, she showed how to calculate the pressure and velocity in both x and y directions in terms of these.

Kemal Sarıoğlu, also made his thesis on this numerical solution of the flow in the pump impellers (Sarıoğlu, 19997). As the domain, he used radial impellers and discretized it by finite volume method. The solution method consists of three-dimensional incompressible Eulerian equations. He obtained several two dimensional analysis for different meridian axis. Thus as a whole he obtained three-dimensional solution.

Ali Aşkın Karakaş, also used a radial impeller discretized by finite volume method (Karakaş, 2000). In his work, the viscous terms of the Navier Stokes equations have been initially eliminated and the equations have been converted into Euler equations type. Then the viscous terms are added again. As the solution domain, the flow between the impeller blades was investigated.

CHAPTER 2

REVIEW OF PUMPS

Pumps are machines that change the energy level of the fluids (Değer, 2005). They can be classified based on applications they serve, the materials they are constructed, the liquids they handle and even their orientation in space. The most basic one is defined by the principle which energy is imported to the fluid (Karassik, 1986). Due to this system, all pumps can be classified in two major categories; dynamic (kinetic) pumps and positive displacement pumps.

A positive displacement pump operates by alternating of filling a cavity and then displacing a given volume of liquid. It delivers a constant volume of liquid against varying discharge pressure or head. The positive displacement pumps can be classified as:

- Reciprocating pumps
- Power pumps
- Steam pumps
- Rotary pumps

Dynamic pumps can be divided into subcategories; centrifugal and other special effect pumps (Karassik, 1986). Centrifugal pumps are basically consists of a stationary pump casing and an impeller mounted on a rotating shaft. It is a kinetic machine that converts mechanical energy into the hydraulic energy through a centrifugal activity such that water enters in axial direction near the shaft is accelerated by revolving impeller blades and finally leaves the pump in circumferential direction (van Esch, 1997).

Selecting between a centrifugal pump and positive displacement pump is not always straightforward. The two types of pumps behave very differently regarding pressure head and flow rate: the centrifugal pump has varying flow depending on the system pressure or head, however, the positive displacement pump has more or less constant flow regardless of the system pressure or head. Positive displacement pumps generally give more pressure than centrifugal pumps'.

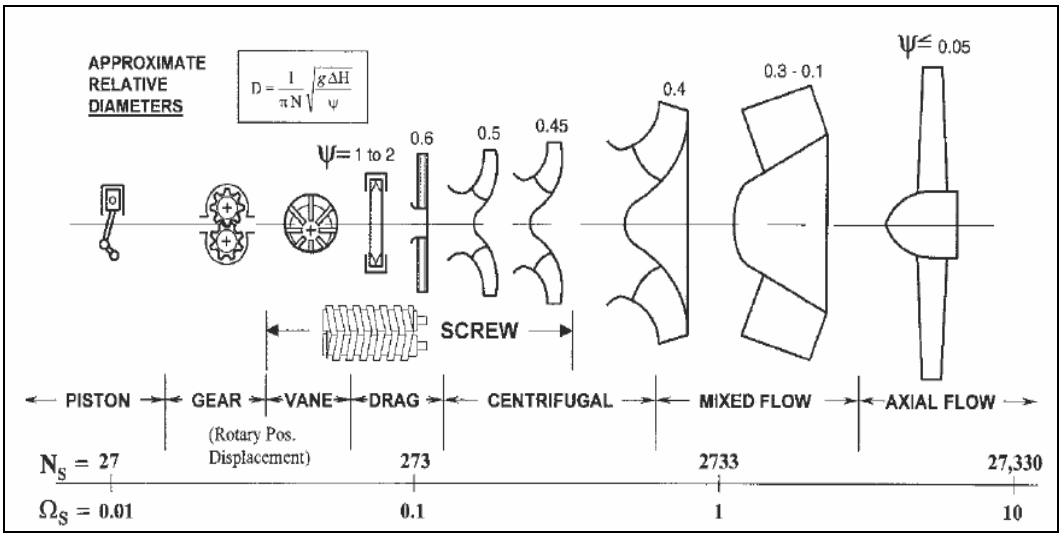

Figure 2.1. Pump classifications due to specific speed (Source: Pump Handbook).

Another major difference between the pump types is the effect of viscosity on the capacity; in the centrifugal pump, the flow is reduced when the viscosity is increased. However, for the positive displacement pump the flow is increased by increasing of the viscosity.

2.1. Historical Review of the Centrifugal Pumps

The invention of the use of centrifugal force as a driving mechanism for pumps was started at the second half of the 17th Century. Initially, problems, like lack of suitable gearing and prime movers of sufficiently high speed and complexity of the efficient centrifugal pump design theory prevent the development and usage of centrifugal pumps at those times. Even after the theoretical work of Euler in 1750, very few understood its principle. However, The Great Exhibition in 1851 became a turning point in the development of the centrifugal pump. Several designs were shown, of which a few appeared to be very successful. Since then the centrifugal pump has developed into a high efficiency machine (van Esch, 1997).

Dennis Papin (1647 – 1712) is believed to be the originator of the centrifugal pump (van Esch, 1997). Although the existence of centrifugal forces was known long before his time, he developed the first proper centrifugal pump as known today: a machine that water enters in axial direction near the shaft, is accelerated by the revolving impeller blades and finally leaves the pump in circumferential direction.

In 1818, the famous “Massachusetts Pump” was introduced in America, which was also a turning point for the development of the centrifugal pump. Its design was similar to the original conception of Denis Papin which the blades running in a circular or spiral casing. From this moment on, the design steadily evolved into the centrifugal pump of today, although departures from previous designs were not always improvements (van Esch, 1997).

2.2. Centrifugal Pumps

Centrifugal pumps are widely used for various types of applications in the industry, irrigation, fire extinguishing, water network systems etc. They have a key position in all watering applications. They have high reliability and stability.

Every centrifugal pump consists of two principal parts: an impeller, which forces the liquid into a rotary motion by impelling action and the diffuser, which directs the liquid into the impeller and leads it away under a higher pressure.

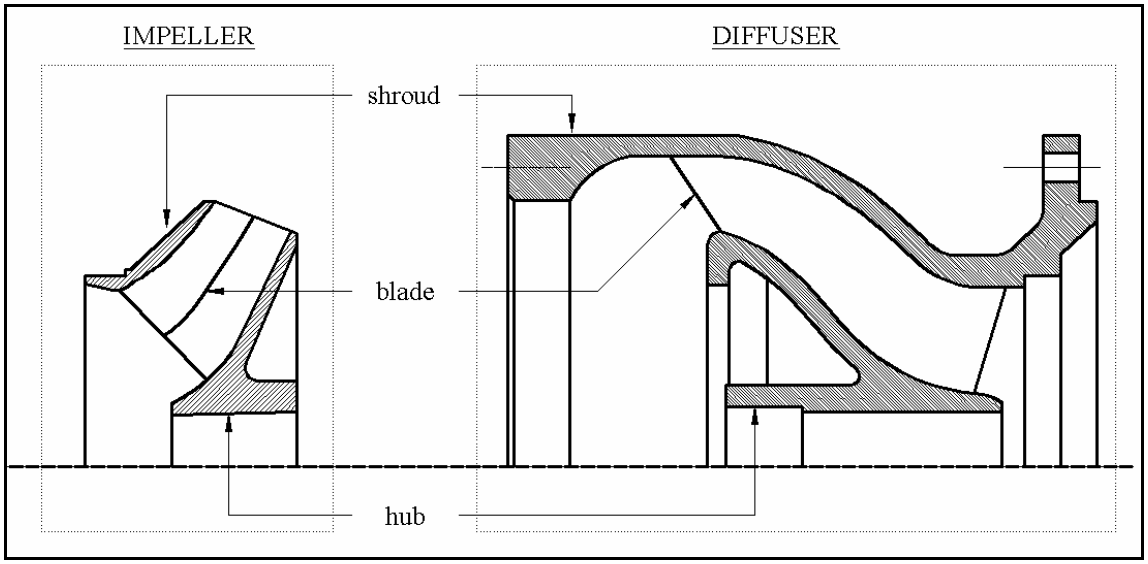

Figure 2.2. The impeller and diffuser of a centrifugal pump.

The impeller, attached on a spinning shaft, is the heart of the centrifugal pump. It contains several blades or vanes, which are always curved backwards. The blades may be of single or double curvature (twisted suction ends). All impeller pumps are rotodynamic, including those with radial flow, mixed flow and axial flow impellers: the

term “centrifugal pumps” tends to encompass all rotodynamic pumps. These types are classified due to blade shapes:

- Radial flow pumps with generally low mass flow rates, high-pressure output and lower efficiencies. The blades of the radial flow pumps are parallel to the pump shaft.
- Mixed flow pumps with wide range of flow, medium range head and high efficiencies. The blades of the mixed flow pumps have curvatures.
- Axial flow pumps with high mass flow rates, low head and high efficiencies. The blades of the axial flow pumps are nearly perpendicular to the pump shaft. The sections of a blade are composed of different airfoil profiles.

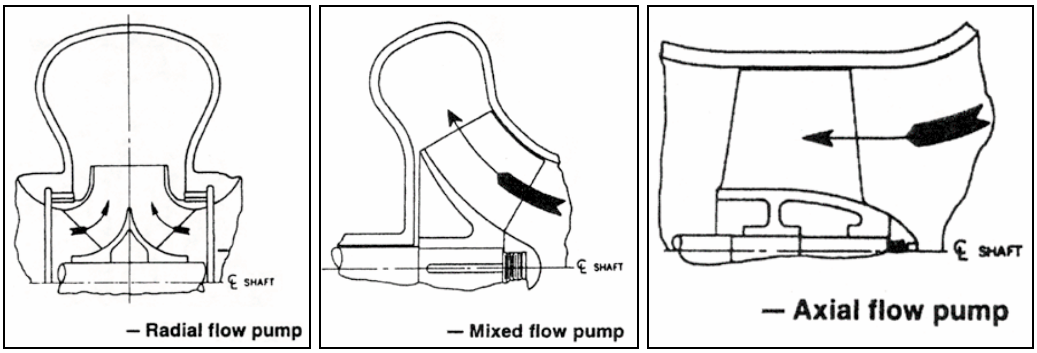

(a) (b) (c)

Figure 2.3. The centrifugal pumps types: a) Radial flow pump, b) Mixed flow pump, c) Axial flow pump (Source: Karassik, 1986)

Centrifugal pumps can be single stage with one impeller, or multi stages with several impellers in series. Each impeller raises the pressure, so the total pressure rise is the sum of those.

Due to the arrangements of the impeller, the centrifugal pumps can be divided into four groups (Karassik, 1986):

- Overhung impeller pumps have their single impellers mounted on the shaft without any bearings horizontally.

- Pumps that have their impellers between bearings, that the impellers are mounted on a shaft that is supported by the bearings and driven through a flexible or rigid coupling by a driver.
- Vertically suspended impeller pumps, which are also called vertical turbine pumps. These pumps have no bearings.
- Magnetically suspended impeller pumps; the impeller is suspended by a magnetic bearing, therefore providing contact free rotation of the impeller inside the pump. They are also known as blood pumps.

The discharge region of the pump, can be a volute or a diffuser, collects the fluid as it leaves the impeller. The cross sectional area of that region is increasing such that high velocity of the fluid is partly converted to the static pressure; in other words, the dynamic head (velocity head) is converted to the static head.

The pump casing has to be packet around the shaft to prevent external leakage. Closely fitted rings, called wearing rings, are mounted on the impeller and fitted in the casing to restrict leakage of high-pressure liquid back to the pump suction. Liquid is directed to the impeller eye by the suction nozzle and is brought into a circular motion by the impeller vanes.

Centrifugal pumps are high efficiency machines, which also can be adapted to suit almost any working condition.

2.3. Definitions

A pump has three main parameters that define its characteristic: the rotation speed, the head and the mass flow rate.

The total head, H_T of a pump is defined as the height (in meters) which the pump can lift a fluid. It includes the velocity head, and the elevation height at the point of interest. The static head, however, is related with the increase in total pressure p_s of the fluid by:

$$H = \frac{p_s}{\rho g} \tag{2.1}$$

where ρ is the density of the fluid raised and g is the gravitational constant.

The head is reversely proportional to the flow rate. However, as in the Figure 2.4, due to the recirculation, shock and friction losses, the actual head flow curve is much lower than the expected one.

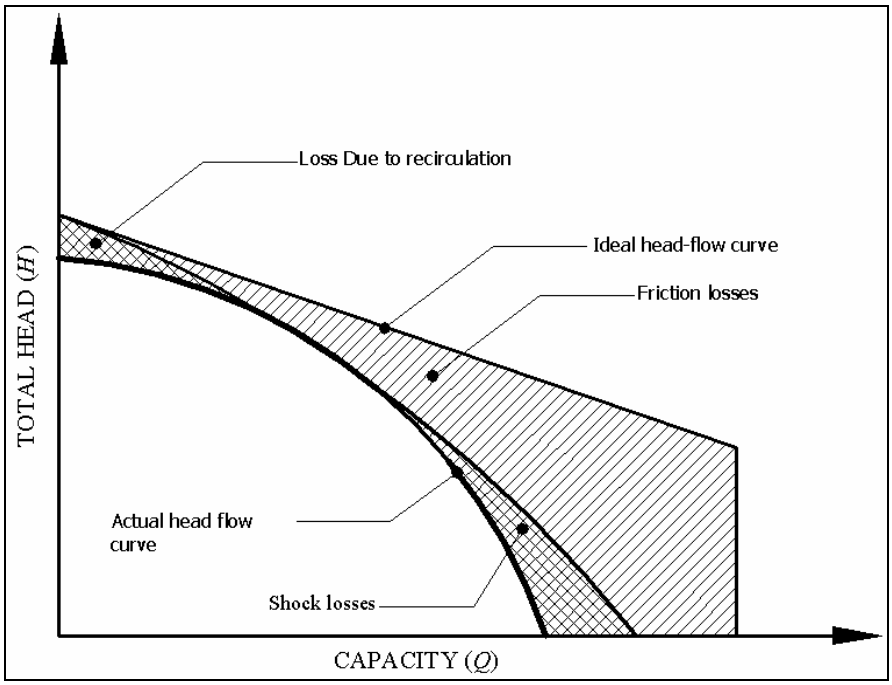

Figure 2.4. The head flow curve.

Unfortunately, due to the first law of thermodynamics, the power applied can not be transferred to the liquid without any losses. Several sources for energy losses can be identified. The most important are mechanical losses in shaft bearings, losses attributed to leakage, disc friction losses and hydraulic losses resulting from roughness, turbulence, boundary layer separation, mixing processes etc. The overall efficiency η is defined as the ratio of the pumps energy output to the power input applied at the shaft. In terms of delivered head H the overall efficiency can be written as

$$\eta = \eta_{hyd.}\eta_{mech.}\eta_{other} = \frac{\rho g Q H}{P_{shaft}} \tag{2.2}$$

where Q is the mass flow rate and P_{shaft} is the shaft power. A convenient means of presenting the overall performance of a specific pump is the use of characteristic curves.

For any centrifugal pump, curves can be developed to show the relationship between flow head, power, efficiency, and net positive suction head. Variation of the head with capacity at a constant speed is called the pump characteristic. The characteristic curves indicate the behavior of a pump under changing operating conditions. At such a curve the head, power input and efficiency at constant speed are plotted against the flow rate. The flow rate for which the efficiency is highest is called the best efficiency point (BEP) (Figure 2.5).

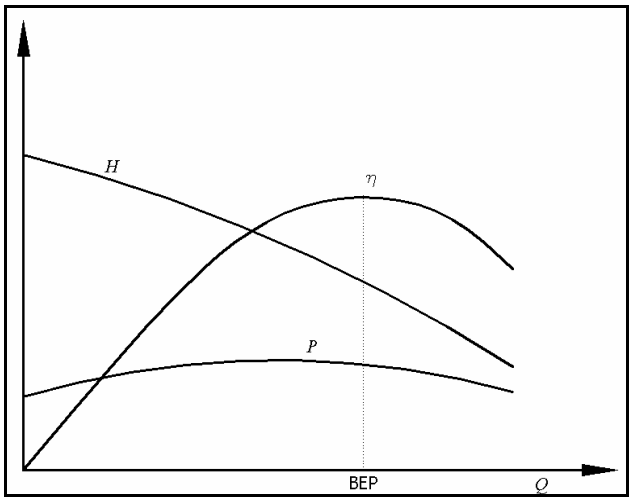

Figure 2.5. A simple pump characteristic curve.

Since the operating principle is based on the centrifugal forces, rotation speed is the one of the most important parameter of the pumps. Head and capacity of a pump vary with the speed in such a way that the performance curves retain their characteristic features. The variation of head, capacity, and power with speed follows definite rules known as affinity rules. When applied to every point on the head – capacity curve, these laws state: when rotation speed is changed, capacity varies directly as the speed, the head varies directly as the square of the rotation speed, and the power consumed varies directly as the cube of the rotation speed. The cube of the rotation speed is based on the assumption that efficiency stays constant with speed for each point (Stephanoff, 1957). The affinity laws can be expressed by the following equations:

$$\frac{n_1}{n_2} = \frac{Q_1}{Q_2} = \left(\frac{H_1}{H_2}\right)^{1/2} = \left(\frac{P_1}{P_2}\right)^{1/3} \tag{2.3}$$

where n is the rotational speed.

These affinity rules are results of dimensional analysis of Stephanoff in 1964, which reveals the existence of several scaling laws for groups of geometrically similar machines. He defines dimensionless specific speed as;

$$n_\omega = \frac{nQ^{1/2}}{(gH)^{3/4}} \tag{2.4}$$

where n_ω is the specific speed, can also be accepted as the identity card of a pump. According to its definition, geometrically similar machines with similar internal flow conditions have the same specific speed value. Depending on the specific speed, the slope of the head characteristic varies from flat (low specific speed) to steep (high specific speed).

Characteristics of centrifugal pumps are said to be stable when the head curve rises steadily, such as there is always a negative slope in relation to the Q axis. For every head, there is a single flow rate. Pumps with low specific speeds and large angles of incidence are prone to instability. Axial flow pumps (high specific speed) with adjustable impeller vanes have an instability range within which it is not permissible to operate them.

CHAPTER 3

PUMP TESTS

Numerical analyses are useless unless the results are compared with the actual test results. The comparison gives the accuracy of the numerical analysis and validates the employed coefficient such as the verification for the mesh, the coefficients used, and the solution method. If the results matched within a specific tolerance, the other obtained results, which can not be measured by tests, can be accepted true and evaluated. For such a comparison, the pump tests must also have high accuracy and precision. The calibration of the measurement equipment must be done, and the tests must be conducted due to the specified standards.

The test of the pump is important due to the many reasons such as; to find the pump performance, to optimize the impeller diameter, to find the effect of special materials on the performance and for several other reasons. During pump a test, the mass flow rate, head, and pump inlet energy are the main parameters, which should be measured (Değer, 2004).

The pump, investigated in this study, has been tested by Duymuş in the calibrated test stand of Vansan Company and the characteristic curve has been obtained. The numerical results of the present study are compared with the experimental study of Duymuş.

It might be useful to briefly explain the test stand in which the experimental study of Duymuş has been performed. The test stand has magnetic flow meters, pressure transmitters, power analyzers, and a network system. The signals of measuring devices are collected by a data acquisition card and are processed by a computer program.

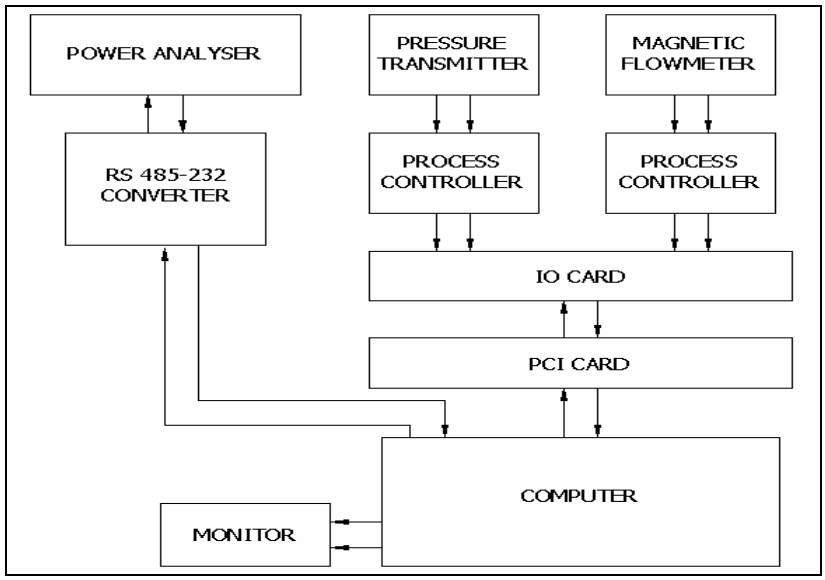

Figure 3.1. The data acquisition schematic view.

The test mechanism is built on a test pool and controlled via the control room (Figure 3.2). In order to process the data received, an interface program is used. This program, basically, analyzes the input data, eliminates the distortions and calculates the averages of the measured values.

Figure 3.2. The flow meters, pressure transmitters, and the linearly controlled valves in the test process.

There are inevitable errors in the used digital equipments. Due to their catalogue data, the power analyzer has ±0.3 %, pressure transmitters have ±0.5 %, and mass flow meters have ±0.5 % error in their measurements.

In order to measure pressure, pressure tapings are used. They are located 3 pipe diameters after the pump discharge in order to comply with the ISO 3555 standard. The mass flow rate is controlled by the valve, in front of the flow meter, after the pressure transmitter. So for different mass flow rates, the characteristic of the pump can be obtained.

The power analyzer is connected to the motor panel of the pump. It can measure almost all parameters about the energy consumed by the motor. This value is multiplied with the motor efficiency that can be obtained from the motor catalogue. So the power that pump consumes can be calculated:

$$P_{PUMP} = P_{MOTOR} \times \eta_{MOTOR} \tag{3.1}$$

As mentioned before, for the validation of a test, the test stand must fit the conditions which are described in standards. The ISO 5198 standard defines the minimum pipe length that must be used before and after the flow meter; that is a minimum of 10 times of pipe diameter for the inflow and a minimum of 5 times the pipe diameter for the outflow.

Briefly, by changing the water mass flow rate, the head and the power for the pump is measured and the efficiency of the pump is calculated. After obtaining the experimental values, the characteristic curve of the pump for the specified rotation is plotted.

CHAPTER 4

THE CONSIDERED PROBLEM

4.1. General Information

The pump which is considered in this study is a semi axial centrifugal pump that consists of closed impellers and a diffuser. It is a submersible type which is widely used for well applications. It is a vertical turbine pump that was designed for 14" wells and 120 kg/s flow rate. Practically, a suction case for the inlet and a discharge for the outlet are mounted on the pump. According to the required head, these stages are connected serially on a shaft. In order to increase the head for a constant flow rate, more stages are added to the pump. The investigated pump is the product of VANSAN Company and coded as VDP 1433. More information about the pump can be obtained from VANSAN Company (http://www.vansan.com.tr).

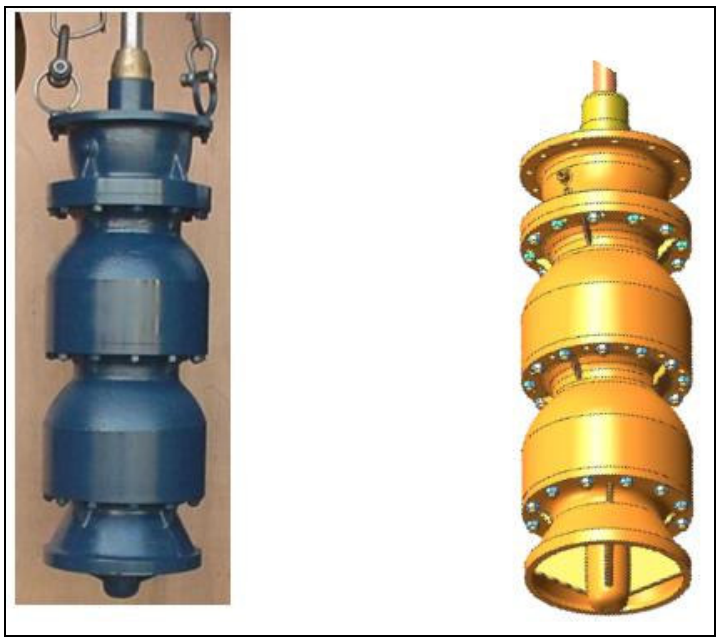

Figure 4.1. VDP 1433 with two stages and its CAD model.

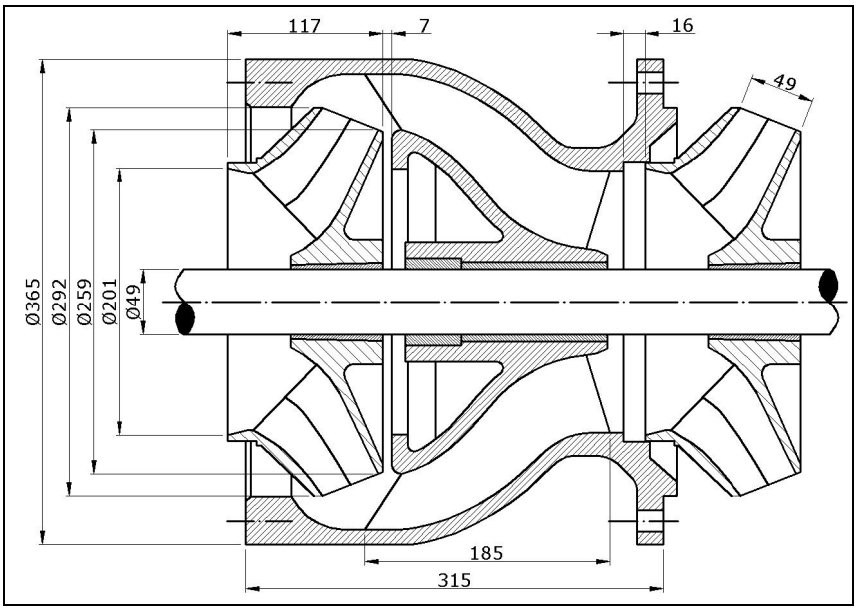

Figure 4.2. The sectional view of the assembled pump with main dimensions.

4.2. Specifications

A general view of a single stage is shown in Figure 4.2. The diffuser has seven blades and the impeller has six blades. The diffusers are designed such that to increase the static pressure at the outlet of the pump.

The diffusers and impellers are produced by casting method. Their materials are usually cast iron, however they can also be manufacturing from bronze. It should be also noted that, before the installation of the pump parts, the inner surfaces of the impeller and the diffuser are polished and so the surface roughness is decreased. Some specific dimensions of the pump as specified in Figure 4.2 are as follows:

Maximum diameter of pump : 365 mm
The height of the diffuser : 315 mm
Impeller diameter : 292 mm

In order to start the numerical procedure, the fluid model of the pump is required. From the solid model of the pump, the fluid model was obtained as seen in Figure 4.3. This model also contains the impeller fluid, which is rotating, and the stationary diffuser part.

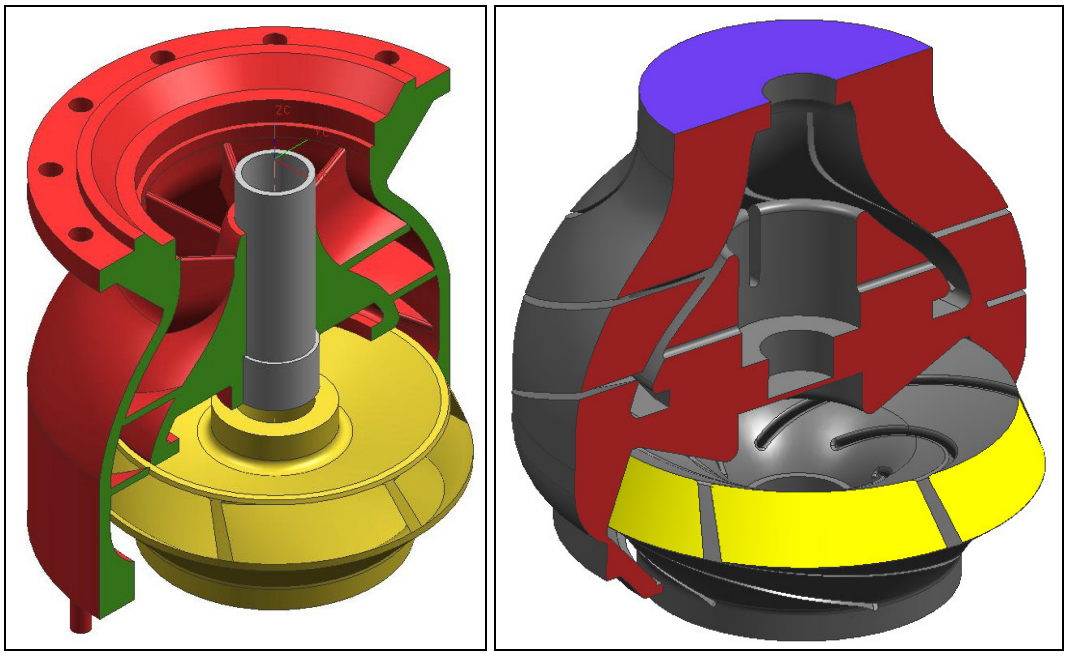

(a) (b)

Figure 4.3. The solid and fluid model of the pump (the diffuser is sectioned for better view).

Apart from the geometry, a pump is best described by its performance curve. The speed of the considered pump is 1450 rpm. As seen from the chart, the best efficiency point of the pump is at 120 kg/s, and at this point, the head is approximately 160 kPa. The characteristic curve of the pump is shown in Figure 4.4.

Table 4.1. The test values of a single stage VDP 1433.

Head	Capacity	Power Consumed	Hydroulic Power	Efficiency
mWC	kg/s	kW	kW	%
26.95	0	19.2	0.0	0.0
22.2	47.8	19.7	10.4	52.8
20.25	74.7	20.5	14.8	72.3
18.3	93.4	21.35	16.8	78.5
16.3	113.9	21.95	18.2	82.9
15.35	124.8	22.35	18.8	84.0
14.35	131.5	22.35	18.5	82.8
13.35	137	22.25	17.9	80.6
11.4	150.5	21.95	16.8	76.6
9.45	162.3	21.1	15.0	71.3
7.45	174.3	20.3	12.7	62.7

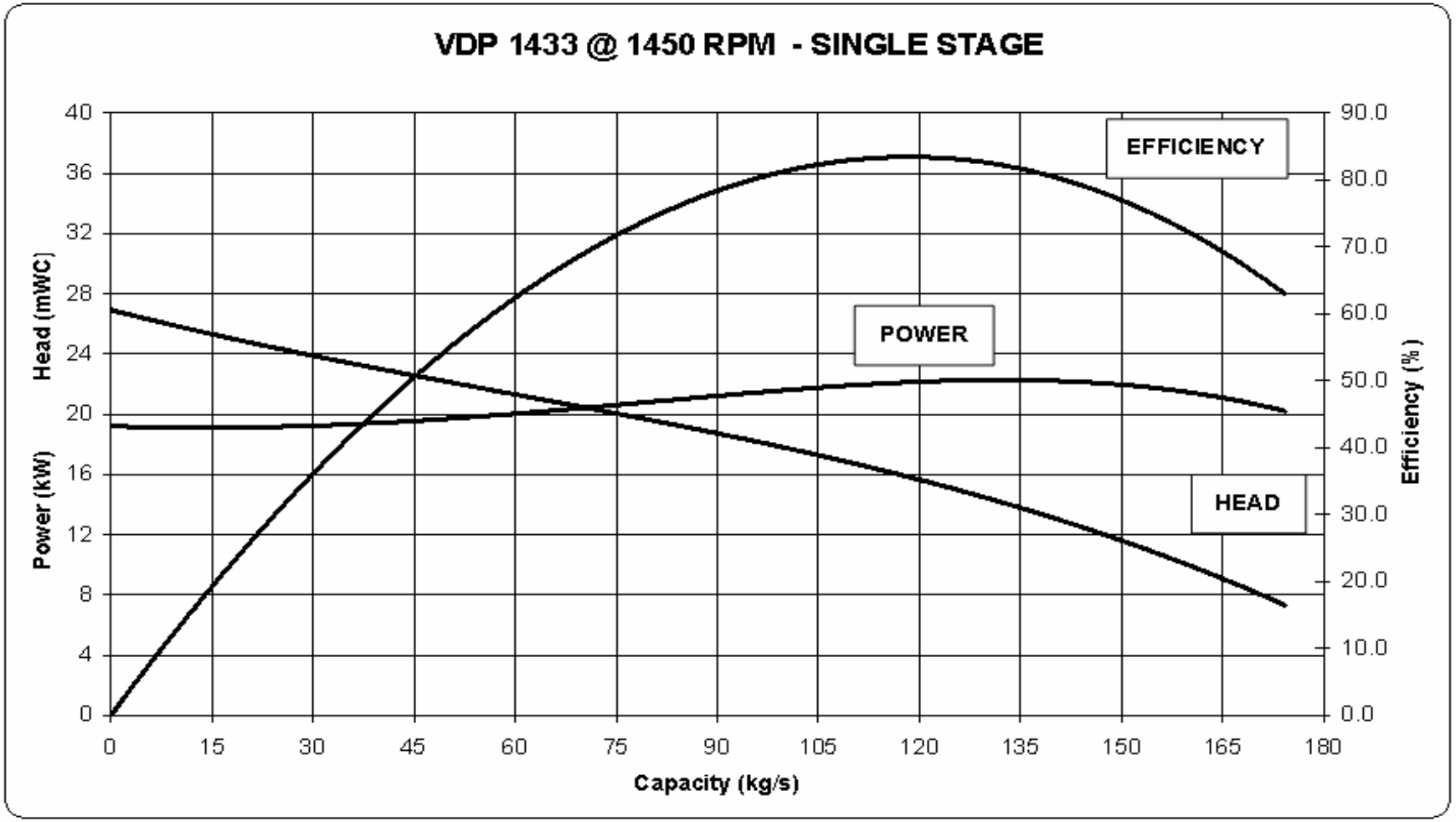

Figure 4.4. The characteristic curves of VDP 1433 at1450 RPM

CHAPTER 5

INTRODUCTION TO CFD

CFD is the analysis and simulation of fluid flow by the mathematical models within the given conditions (Ferziger, 2002). This provides to understand the physical events that occur in the flow of fluids around and within designated objects. Those fields are governed by the equations of the fluid mechanics, chemical reactions, and the related phenomena are nonlinear which often have no analytical solutions. So instead, numerical methods with acceptable truncation errors are used.

These simulations require many computations, which mean high computational sources and complex softwares. With the increasing computer technology and industrial demand, by a qualified analyst, these flow modeling softwares can be used to create a virtual prototype of the product or process that simulates the real world conditions. The advantages of the CFD can be listed as (Lomax, 1999):

- Substantial reduction of lead times and costs of new designs
- Ability to study systems where controlled experiments are difficult or impossible to perform (e.g very large systems)
- Ability to study systems under hazardous conditions and at beyond their normal performance limits (eg safety studies and accident scenarios)
- Practically unlimited level of detail of results.

In order to perform a meaningful CFD design analysis, four main elements must be incorporated into the method.

1. Goal definition – what are the objectives? How will they be measured?
2. Domain and material definitions – CAD representation of the domain, physical properties for fluid and solids (if modeled)
3. Boundary condition definitions – are conditions time dependent? What kinds of boundaries exist? (wall, inlet, outlet, mass flow, pressure etc). Can the conditions represent the actual conditions?

4. Iterative development plan – how will the analysis be performed.

The first step of a CFD analysis involves the specification the problem and governing parameters. The CAD representation of the domain and the material properties for fluids and solids should be given. Then this geometry of interest is divided, or discretized, into a number of computational cells. Discretization is the method of approximating the differential equations by a system of algebraic equations for the variables at some set of discrete locations in space and time. The discrete locations are referred to as the grid or the mesh. Then the problem is specified and an appropriate set of governing equations and boundary conditions must be selected. If required, the appropriate turbulence model should be specified. Then, the iterative development plan of the performed analysis is stated. Finally, after completing the sufficient number of iterations, the results of the simulation must be commented and interpreted. This step can require post-processing of the data and can be done by flow visualization tools like colorful and error estimation techniques.

The most important part of a CFD is, the results can not be evaluated without experimental validation.

There are many possible sources of error in a CFD analysis, as summarized below:

1. Discritization error.
2. Machine truncation error.
3. Mesh related errors such as the lack of resolution (number and skewness of elements) and the approximation of the boundary geometry.
4. Stability enhancers such as artificial viscosity.
5. Approximations of the flow physics by simplified models (turbulence)
6. Computational error such as stalled convergence.

As seen above, the magnitude of the discretization error depends upon both the order of discretization and the size of the elements.

CHAPTER 6

GOVERNING EQUATIONS

6.1. General Form of the Governing Equations

There are three main equations valid for a flow inside a control volume;

a. Continuity equation which is a scalar equation and describes the conservation of mass

b. Momentum equations, which are vectoral equations, are derived based on Newton's second law of motion: the changes of momentum for a control volume in a finite time interval are equal to the sum of all applied forces to the control volume. The continuity and the momentum equations are also called as Navier-Stokes equations

c. Energy equation, which is a scalar equation, defines the conservation of energy.

These equations in their general forms can be listed as;

$$\frac{\partial \rho}{\partial t} + \vec{\nabla}.\rho\vec{V} = 0 \tag{6.1}$$

$$\frac{\partial \rho\vec{V}}{\partial t} + \vec{\nabla}.(\rho\vec{V})\vec{V} = -\vec{\nabla}p + \vec{\nabla}.\tau + F_{BODY}.\vec{r} \tag{6.2}$$

$$\rho\frac{\partial h}{\partial t} + \vec{V}.\vec{\nabla}h = \vec{\nabla}(k\vec{\nabla}T) + \frac{\partial p}{\partial t} + \vec{V}.\vec{\nabla}p + (\tau.\vec{\nabla})\overline{V} + S \tag{6.3}$$

where ρ is the density, $\vec{V}$ is the velocity vector, p is the pressure, τ is the stress, F_{BODY} is the body forces (external forces), h is the total enthalpy, T is the temperature, k is the thermal conductivity, and S as the external source.

6.2. Assumptions for the Considered Flow

For most fluid flow problems, these equations are too complicated to be solved either analytically or numerically. In the case of a flow through a hydraulic pump operating near design condition, the used mathematical equations can be simplified considerably without losing its overall validity. The following assumptions can be accepted in order to obtain more convenient and simplified form of the governing equations:

6.2.1. Isothermal Flow

Temperature inside the pump is not changed with time and fluid flows at a constant temperature. Thus, the fluid flow through a centrifugal pump is essentially isothermal. Heat generation due to viscous forces and heat transfer between pump and surroundings are negligible. Even if the process is not isothermal, the density of a liquid weakly depends on the temperature. For the present problem, the temperature of the flow is not changed and the flow is considered as isothermal. Thus, the terms in the general form of the governing equations (Eq. 6.1 to 6.3) that contain variation of temperature and enthalpy are neglected. The energy equation is excluded from the governing equations and will not be solved for the present problem.

6.2.2. Incompressible Newtonian Fluid

Flows, in which variations of density are negligible, are defined as incompressible; when the density variations within a flow are not negligible, the flow is called compressible. Compressible flows occur frequently in engineering applications. Compressibility effects are very important in the design of modern high speed aircraft and missiles, power plants, fans, compressors etc.

Actually incompressible fluid is a thermo dynamical term; however incompressible flow is a term of fluid mechanics. These two terms are different from each other and should not be confused. The motion of a compressible fluid can be assumed as incompressible (Sarıoğlu, 1997). The main criterion for the incompressible

flow is the Mach number (M); for M<0.3, the maximum density variation is less than 5%, therefore the flow can be treaded as incompressible.

As defined before, incompressible flow is the flow that the substantial change in the density of the fluid particles with respect to time can be negligible. This can be modeled from the continuity equation as,

$$\frac{1}{\rho}\frac{D\rho}{Dt} = 0 \tag{6.4}$$

For the present study, density of the all the fluid particles can be assumed same and is not changed through space and time. Thus, for an incompressible flow since the density is not changed and is constant, the general form of the governing equations become as:

$$\vec{\nabla}.\vec{V} = 0 \tag{6.5}$$

$$\frac{\partial \vec{V}}{\partial t} + \vec{\nabla}.(\vec{V})\vec{V} = -\frac{1}{\rho}\vec{\nabla}p + \frac{1}{\rho}\vec{\nabla}.\tau + \frac{1}{\rho}F_{BODY}.\vec{r} \tag{6.6}$$

As is seen from the above equations, density is constant and is taken out of derivatives.

All real fluids have internal friction, so their rate of deformation is a function of the applied shear stress. If the rate of deformation is directly proportional to the applied shear stress, the fluid is called Newtonian fluid. For the Newtonian fluids the stress terms are defined based on the velocity components. Thus, for an incompressible Newtonian fluid the governing equations can be written as:

$$\vec{\nabla}.\vec{V} = 0 \tag{6.5}$$

$$\vec{\nabla}.(\vec{V})\vec{V} = -\frac{1}{\rho}\vec{\nabla}p + \nu\vec{\nabla}^2 V + \frac{1}{\rho}F_{BODY}.\vec{r} \tag{6.7}$$

In the present study, the governing equations are solved for water at 20°C. As known, water is a Newtonian and incompressible fluid. Thus, the general form of the continuity and momentum equations (Eq 6.1 and 6.2) are simplified to Eq 6.5 and 6.7.

6.2.3. Turbulent Type Flow

The flow inside the pump is internal turbulent type. Flows, which are bounded by solid surfaces, are called internal flows. Internal flows include flows through pipes, ducts, nozzles, diffusers, sudden contractions and expansions, valves and fittings. These flows may be laminar or turbulent.

All flows encountered in engineering practice become unstable above a certain Reynolds number. At low Reynolds numbers flows are laminar however as the Reynolds number increases; flows are observed to become turbulent. A chaotic and random state of motion develops in which the velocity and pressure change continuously with time within substantial regions of flow. Obviously, the flows in turbo machines are mainly turbulent due to high velocities.

Direct calculation of a basic turbulence situation needs a huge amount of computational source and time. Since it is difficult to solve turbulent flows directly, some basic models are used instead. These models are usually obtained by adding a shear stress term, which expresses the turbulence, to the laminar viscous stress:

$$\mu_{eff} = \mu + \mu_t \tag{6.8}$$

where μ_t and μ_{eff} are turbulence and effective viscosity respectively. As seen, the effective viscosity includes both dynamic and turbulence viscosity. Actually, the kinematic viscosity is the property of the fluid; however, turbulence viscosity is the feature of the flow.

Turbulent flow and turbulence models will be examined in details in the next chapter. In this study, $k-\varepsilon$ turbulence model is mainly used and the governing equation for this model can be described as:

$$\frac{\partial}{\partial t}(\rho k) + \frac{\partial}{\partial x_i}(\rho k u_i) = \frac{\partial}{\partial x_j}\left[\left(\mu + \frac{\mu_t}{\sigma_k}\right)\frac{\partial k}{\partial x_j}\right] + G_k + G_b - \rho\varepsilon - Y_M + S_k \tag{6.9}$$

$$\frac{\partial}{\partial t}(\rho\varepsilon)+\frac{\partial}{\partial x_i}(\rho\varepsilon u_i)=\frac{\partial}{\partial x_j}\left[\left(\mu+\frac{\mu_t}{\sigma\varepsilon}\right)\frac{\partial\varepsilon}{\partial x_j}\right]+C_{1\varepsilon}\frac{\varepsilon}{k}(G_k+C_{3\varepsilon}G_b)-C_{2\varepsilon}\rho\frac{\varepsilon^2}{k}+S_\varepsilon \quad (6.10)$$

6.2.4. Three Dimensional Flow

The modeled pump geometry and the fluid volume inside this geometry are three-dimensional. There might be some studies in literature in which the flow inside a pump has been studied as two-dimensional. Foe example the flow inside a radial pump impeller can be investigated in two-dimensional. However, for the selected pump, which is a semi axial pump, the velocity vectors for all dimensions are important and have directly effects on the required results. Therefore, the problem should be handled in three-dimensional coordinate systems.

6.2.5. Symmetric Geometry Position

Although the impeller rotates and the position of the impeller blades with respect to diffuser blades changes with time, the modeled flow for a specific position is solved. However, the geometry can be regarded as same for all other positions. Although the transfer of the energy to the fluid by rotating blades is unsteady, the flow across the boundaries of a control volume surrounding the pump can be considered as steady flow. So the problem is solved for a fixed impeller and diffuser position. Since the flow is considered as at steady state, the terms, which have time variables in the general form of governing equations, will be omitted.

6.3. Proper Form of Governing Equations for Pumps

Based on the all information given above and assumptions for the present flow, the governing equations for the problem which are continuity, momentum, k and e equations can be written as:

$$\vec{\nabla}.\vec{V}=0 \quad (6.5)$$

$$(\vec{\bar{V}}\vec{\nabla})\vec{\bar{V}} = -\frac{1}{\rho}\vec{\nabla}\bar{P} + \nabla\left[(\nu + \nu_t)\nabla\ \vec{\bar{V}}\right] \tag{6.11}$$

$$\frac{\partial}{\partial x_i}(\rho k u_i) = \frac{\partial}{\partial x_j}\left[\left(\mu + \frac{\mu_t}{\sigma_k}\right)\frac{\partial k}{\partial x_j}\right] + G_k + G_b - \rho\varepsilon - Y_M + S_k \tag{6.12}$$

$$\frac{\partial}{\partial x_i}(\rho \varepsilon u_i) = \frac{\partial}{\partial x_j}\left[\left(\mu + \frac{\mu_t}{\sigma\varepsilon}\right)\frac{\partial \varepsilon}{\partial x_j}\right] + C_{1\varepsilon}\frac{\varepsilon}{k}(G_k + C_{3\varepsilon}G_b) - C_{2\varepsilon}\rho\frac{\varepsilon^2}{k} + S_\varepsilon \tag{6.13}$$

CHAPTER 7

TURBULENCE AND ITS MODELLING

Almost all-fluid flow that is encountered in daily life is turbulent. Typical examples are flow around cars, airplanes and buildings. The flow and combustion in engines, both in piston engines and gas turbines and combustors, are highly turbulent. Air movements in rooms are also highly turbulent.

At values of Reynolds number above Re_{crit} a complicated series of events takes place, which eventually leads to a radical change of the flow character. The velocity and all other flow properties vary in a random and chaotic way. This regime is called turbulent flow.

7.1. Turbulent Flow Characteristics

Turbulent flow is irregular, random and chaotic. Even tough turbulence is chaotic, it is deterministic and is described by the Navier Stokes equations.

In turbulent flow the diffusivity increases. This means that the spreading rate of the boundary layers, jets, etc. increases as the flow becomes turbulent. The turbulence increases the exchange of momentum in e.g. boundary layers and reduces or delays thereby separation at bluff bodies such as cylinders, airfoils and cars. The increased diffusivity also increases the resistance (wall friction) in internal flows such as in channels and pipes.

Turbulent flow is always three-dimensional. It is dissipative, which means that kinetic energy in the small (dissipative) eddies are transformed into internal energy. The small eddies receive the kinetic energy from slightly larger eddies and so on. The largest eddies extract their energy from the mean flow. This process of transferred energy from the largest turbulent scales to the smallest is called cascade process (Davidson, 2003).

Even though there are small turbulent scales in the flow, they are much larger than the molecular scale and can be treated as a continuum.

The effects produced by turbulence may or may not be desirable, depend on the application. Intense mixing is useful when chemical mixing or heat transfer is needed;

both of these may be increased by the orders of magnitude by turbulence. On the other hand, increased mixing of momentum results in increased frictional forces, thus increasing the power required to pump a fluid or to propel a vehicle; again, an increase by an order of magnitude is not unusual.

7.2. Turbulence Modeling

As mentioned before, the velocity and all other characteristics vary in a random way in turbulent flow. Therefore, modeling turbulent flow directly (direct numerical solution) requires using very small scales and a very fine resolution in time (since the turbulent flow is always unsteady). However small scales mean more calculations and high computer sources that are still not available today for modeling this amount of turbulence. So, in order to show the effect of the turbulent flow in a steady flow analysis, by using the mentioned characteristics, a turbulent viscosity term is introduced. This term is calculated from the other properties and shows its effect as viscosity increase in the equations.

Modeling turbulence starts with velocity component which can be decomposed into a steady mean value V with a fluctuating component $v'(t)$ superimposed on it;

$$V(t) = V + v'(t) \tag{7.1}$$

In general, it is most attractive to characteristic turbulent flow by the mean values of flow properties (*U, V, W, P etc*) and the statistical properties of their fluctuation (*u', v', w', p', etc*). One reason why these variables are decomposed is that when the quantities are measured the mean values are more important and interested than the time histories.

These time-averaged variables modify the governing equations which contains additional unknown variables. For different types of flow, determining these variables in terms of known quantities requires different turbulence models.

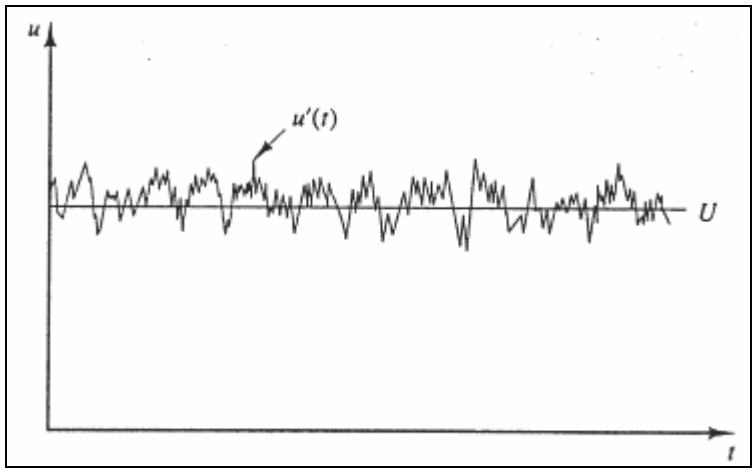

Figure 7.1. The velocity measurement in turbulent flow.

7.3. Types of Turbulence Models

No turbulence model is universally accepted as being superior for all types of problems. The choice of the turbulence model will depend on considerations such as the physics encompassed in the flow, established practice for a specific class of problem, the level of accuracy required, the available computational resources, and the amount of time available for simulation.

An algebraic model equation is used to compute a turbulent viscosity, often called eddy viscosity. The Reynolds stress tensor is then computed using an assumption, which relates the Reynolds stress tensor to the velocity gradients and the turbulent viscosity. This assumption is called the Boussinesq assumption. Models that are based on turbulent (eddy) viscosity are called eddy viscosity models.

In one-equation models, a transport equation is solved for a turbulent quantity (usually turbulent kinetic energy) and a second turbulent quantity (usually turbulent length scale) is obtained from an algebraic expression. The turbulent viscosity is calculated from Boussinesq assumption. The two equation models fall into the class of the eddy viscosity models. Two transport equations are derived which describe transport of two scalars, for example the turbulent kinetic energy k and its dissipation ε. The Reynolds stress tensor is then computed using an assumption which relates the Reynolds stress tensor to the velocity gradients and an eddy viscosity. The latter is obtained from two transported scalars.

Above the different types of turbulence models have been listed in increasing order of complexity, ability to model the turbulence, and cost in terms of computational work. Among the mentioned models, $k-\varepsilon$ model (Jones and Launder 1972) has become the popular one for most of applications (Wilcox 1993). It is computationally tractable and robust. In this model, two partial differential equations, one for the turbulent kinetic energy (k) and a second for the rate of dissipation of the turbulent kinetic energy (ε) are solved, where k and ε are defined follows (Wilcox 1993):

$$\rho k = \frac{1}{2}\rho\overline{u_i'' u_i''} \tag{7.3}$$

$$\rho\varepsilon = \tau_{ij}\frac{\partial u_i''}{\partial x_j} \tag{7.4}$$

The transport equation for these properties is presented below:

$$\frac{\partial}{\partial t}(\rho k)+\frac{\partial}{\partial x_i}(\rho k u_i)=\frac{\partial}{\partial x_j}\left[\left(\mu+\frac{\mu_t}{\sigma_k}\right)\frac{\partial k}{\partial x_j}\right]+G_k+G_b-\rho\varepsilon-Y_M+S_k \tag{7.5}$$

$$\frac{\partial}{\partial t}(\rho\varepsilon)+\frac{\partial}{\partial x_i}(\rho\varepsilon u_i)=\frac{\partial}{\partial x_j}\left[\left(\mu+\frac{\mu_t}{\sigma\varepsilon}\right)\frac{\partial\varepsilon}{\partial x_j}\right]+C_{1\varepsilon}\frac{\varepsilon}{k}(G_k+C_{3\varepsilon}G_b)-C_{2\varepsilon}\rho\frac{\varepsilon^2}{k}+S_\varepsilon \tag{7.6}$$

In these equations, G_k represents the generation of turbulence kinetic energy due to the mean velocity gradients. G_b is the generation of turbulence kinetic energy due to the buoyancy. Y_M represents the contribution of the fluctuating dilatation in compressible turbulence to the overall dissipation rate. $C_{1\varepsilon}, C_{2\varepsilon}$ and $C_{3\varepsilon}$ are constants. σ_k and σ_ε are the turbulent Prandtl numbers for k and ε, respectively. S_k and S_ε are source terms that can be defined by the user.

So the turbulent (or eddy) viscosity is:

$$\mu_t = \rho C_\mu \frac{k^2}{\varepsilon} \tag{7.7}$$

where C_μ is a constant. The values of the constants can be listed as:

$$C_{1\varepsilon} = 1.44 \quad C_{2\varepsilon} = 1.92 \quad C_\mu = 0.09 \quad \sigma_k = 1.0 \quad \sigma_\varepsilon = 1.3$$

These default values have been determined from experiments with air and water for fundamental turbulent shear flows including homogenous shear flows and decaying isotropic grid turbulence. They have been found to work fairly well for a wide range of wall – bounded and free shear flows.

7.4. Wall Functions

As mentioned before, flow inside a pump is highly turbulent. This is because of the high velocities and the twisted blade geometries. The flow behavior and turbulence structure at the walls are considerably different from the free turbulent flows in different ways.

Numerous experiments have shown that the near wall region can be largely subdivided into three layers. In the innermost layer, called the "viscous sublayer", the flow is almost laminar, and so the (molecular) viscosity plays a dominant role in momentum and mass transfer. In the outer layer, also called the fully turbulent layer, turbulence plays a major role. Between these two layers, there is an interim region where the effects of molecular viscosity and turbulence have nearly same importance. These regions are plotted on a chart as in Figure 7.2.

In the linear sub layer where the fluid layer in contact with a smooth wall, turbulent eddying motions end near the wall. Therefore, the turbulent shear stress effects are dominated by the viscous shear. At this layer, the shear stress is assumed constant and equal to the wall shear stress throughout the layer.

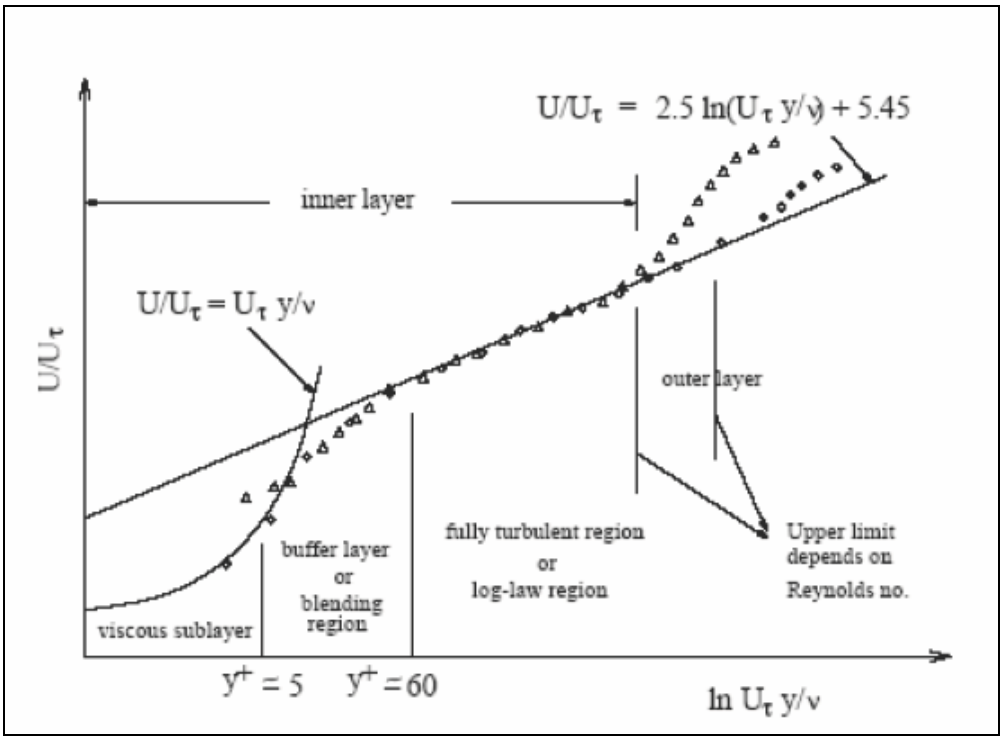

Figure 7.2. The layers at the near wall region (Source: Fluent Users Guide)

The outside of the viscous sublayer where the viscous and turbulent effects are both important, is called the log law layer. Here the shear stress varies slowly with distance from the wall, and within this layer, it is assumed constant and equal to the wall shear stress.

Traditionally, there are two approaches to model near wall region. In the first approach, the viscosity affected inner region (viscous sublayer and buffer layer) is not resolved. Instead, semi empirical formulas called “wall functions” are used to handle the viscosity-affected region between the wall and the fully turbulent region. The use of wall functions overcomes the need to modify the turbulence models for the presence of the walls.

In the second approach however, the turbulence models are enable the viscosity-affected region to be resolved with a mesh all the way to the wall, including the viscous sublayer. For the purposes of discussion, this will be termed the “near wall modeling” approach.

In most high Reynolds number flows, the wall function approach substantially saves the computational resources, because the viscosity affected near wall region in which the solution variables change most rapidly, does not need to be resolved. The

wall function approach is popular because it is economical, robust, and reasonably accurate. It is a practical option for the near wall treatments for industrial flow simulations.

The wall function approach however, is inadequate in situations where the low Reynolds number effects are pervasive in the flow domain in question, and the hypotheses underlying the wall functions cease to be valid. Such situations require near wall models that are valid in the viscosity-affected region and accordingly integrable all the way to the wall.

The standard wall functions in Fluent, which are also used in the present study, are based on the works of Launder and Spalding. It has been most widely used model for industrial flows.

CHAPTER 8

BOUNDARY CONDITIONS

All numerical problems have to be defined within their initial and/or boundary conditions. It is important to correctly specify the boundary conditions in order to obtain realistic results. The type of the boundary conditions that is required by any partial differential equation depends on the physical condition of the problem. Generally, the value of the variable at the boundary (Dirichlet boundary conditions) or its gradient in a particular direction (usually normal to the boundary – Neumann boundary conditions), or linear combinations of the two quantities can be defined. These types of the boundaries will be applied to various surfaces. Some of the used boundary types can be classified as:

- Inlet boundary condition
- Outlet boundary condition
- Wall boundary condition
- Symmetry boundary condition
- Periodicity boundary condition.

For the introduced problem, four types of boundary conditions, namely non – slip stationary wall, non – slip rotating wall, inlet and outlet boundaries exists.

The impeller and diffuser have symmetrical shape and can be considered symmetric individually to simplify the problem. However, as a whole system, since the diffuser and impeller have different number of blades, their position with respect to each other breaks the symmetrical features. For different positioning of the blades, different results are obtained. The periodicity boundary condition is also not suitable for the problem considered.

Figure 8.1 shows the section of the diffuser, impeller and their fluid sections. On the left side of the figure, the types of the boundary conditions applied to the fluid domain can be observed.

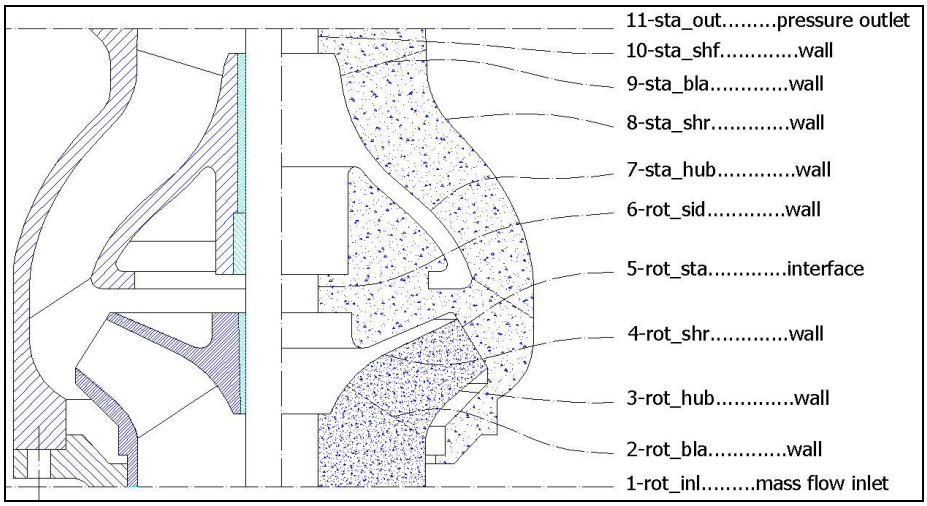

Figure 8.1. The types of the boundary conditions for the considered problem.

8.1. Inlet Boundary Conditions

The inlet boundary condition can be specified by various methods. One of them is to define the pressure at the inlet. The other general one is to specify mass flow at the inlet. For the analysis, the inlet boundary condition is applied at the inlet of the impeller as depicted in Figure 8.2. The velocity vectors are defined as to be normal to this surface. In the present study, all design calculations are performed based on that principle. This definition of inlet boundary condition complies with the practical applications. Practically, a suction case is installed at the inlet of the pump to uniform the flow for impeller inlet.

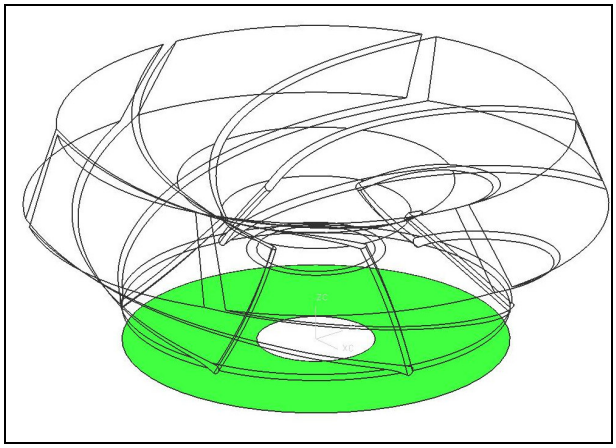

Figure 8.2. The inlet boundary condition is applied to the impeller inlet.

8.1.1. Pressure Inlet Boundary Conditions

Pressure inlet boundary conditions are used to define fluid pressure (total or static pressure) at flow inlets. They are suitable both for incompressible and compressible flow calculations. Pressure inlet boundary condition can be used when the inlet pressure is known but the flow rate and/or velocity is not known. Therefore, the mass flow rate at the inlet is determined due the pressures at the inlet and outlet surfaces. It might be useful to mention that, for a pressure inlet boundary condition, besides the total pressure, the flow direction should also be entered. The total pressure can be defined as:

$$p_0 = p_s + \frac{1}{2}\rho \vec{V}^2 \tag{8.1}$$

where p_0 is the total pressure, p_s is the static pressure, and p_d is the dynamic pressure.

In Fluent program, the flow direction can be specified by either setting the direction vector in any coordinate system or defining normal the direction to boundary surface.

8.1.2. Mass Flow Inlet Boundary Conditions

Mass flow inlet boundary conditions are used to provide a prescribed mass flow rate at the inlet of a fluid volume. Both uniform and non-uniform velocity vectors can be defined at inlet boundary. If non-uniform velocity exists, in addition to magnitude, the distribution vector should also be known. Since the mass flow rate is known, the Fluent program calculates the total pressure from the interior computational solution.

If both the total pressure and the mass flow rate at an inlet are known, the mass flow rate condition is preferred to be employed because the convergence of the pressure inlet solution is much slower with respect to its alternative.

8.2. Pressure Outlet Boundary Conditions

The outlet boundary condition can only be defined by specifying the pressure at the outlet boundary, where the fluid leaves the domain. Pressure outlet boundary conditions require the specification of a static (gauge) pressure at the outlet boundary and all other conditions are extrapolated from the interior of the domain.

As seen from the Figure 8.3, the pressure outlet is defined on the discharge surface of the diffuser. Since the pump shaft passes trough the stage, there is a hole at the center of the boundary, represents the shaft.

If the pressure defined, is higher than the pressure inside the pump, the flow is developed at the reverse direction. In order to model this backflow, a set of backflow conditions should also be specified. The normal velocity can be calculated from the mass flow rate and the inlet area of the geometry.

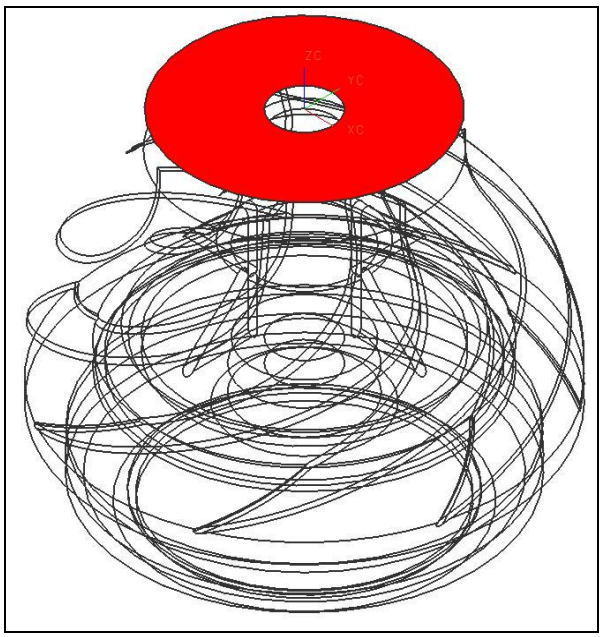

Figure 8.3. The outlet boundary is defined on the discharge of the diffuser.

8.3. Wall Boundary Conditions

Wall boundary conditions are used to bound fluid and solid regions. In viscous flows, the no-slip boundary condition is enforced at walls. All components of the velocity vector at wall boundaries are zero. As shown in Figure 8.4, the blades, hub and

shroud of the both impeller and diffuser can be accepted as the wall boundary condition for the considered problem. The diffuser surfaces are stationary, however, the impeller surfaces rotate at 1450 rpm. For rotating surfaces, a special treatment called “moving reference frame” is employed.

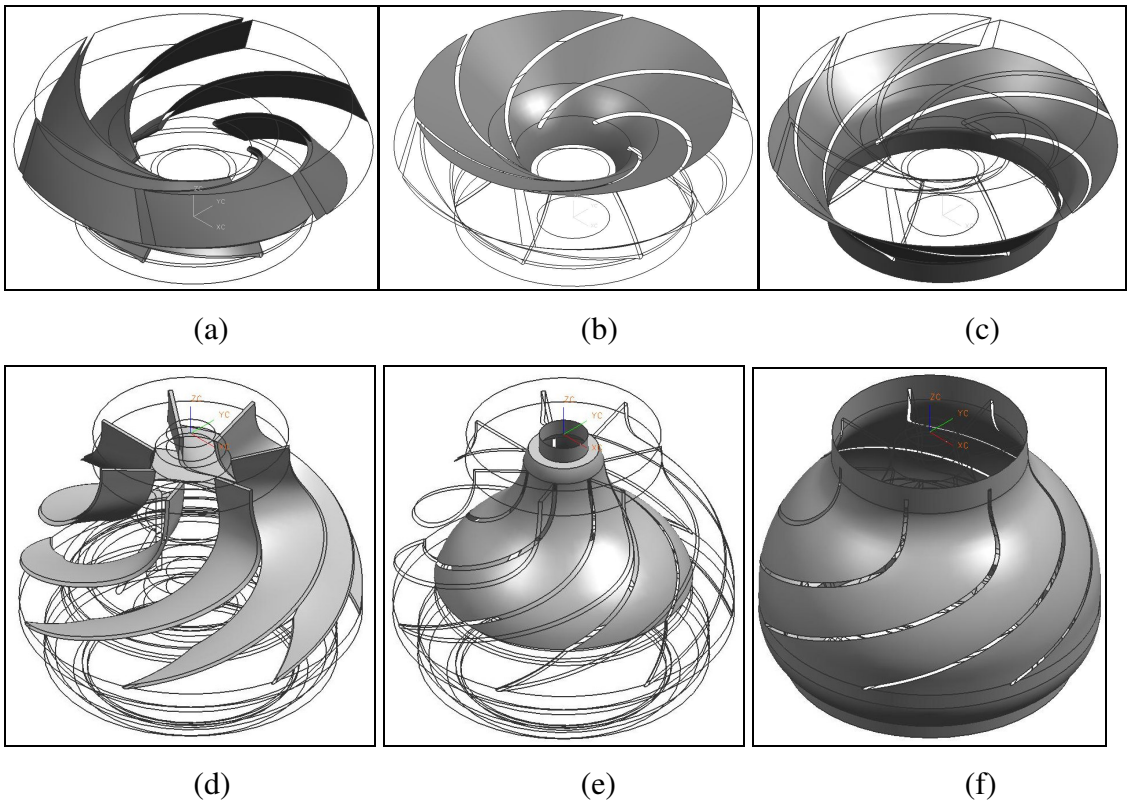

Figure 8.4. The wall boundaries specified for the problem. a) The impeller blades, b) impeller hub, c) impeller shroud, d) diffuser blades, e) diffuser hub, e) diffuser shroud.

8.4. Defining Wall Motion

Wall boundaries can be either stationary or moving. The stationary boundary condition specifies fixed walls, whereas the moving boundary condition can be used to specify the transitional or rotational velocity of the wall, or the velocity components. For rotational motion, the rotation speed (angular velocity) about a specified axis should be specified.

The rotating zone approach consists of two main types. Flows in multiple rotating reference frames, and flow in a single rotating frame as in turbomachinery

applications. In both of the cases, the flow is unsteady relative to a stationary space. Therefore solving a rotating domain problem consists of complex analysis if the angular velocity is directly used. However, if the relative velocity is used instead, the calculations will be simpler. The angular velocity of the rotating domain will be set to zero by defining a rotating space and the flow is steady relative to the rotating (non inertial) frame. Therefore, the computational domain is rendered steady state by considering it rotates with the same speed of the impeller.

This type of treatment provides a stationary domain for the flow inside the rotor. However, if stators are present in addition to a rotor, then it is not possible to render the computational problem steady by choosing the calculation domain that rotates with the rotor or impeller. In other words, for each of the rotating zones and stationary zones, separated domains have to be defined.

There is no doubt the solution between two zones should be matched in order to determine solution for the entire computational domain. In the Figure 8.5 the two fluid zones can be seen separately, also the assembly position is also stated. In such problems, the common surfaces of the both zones that the flow passes through from one to other are called interface surfaces. Since these surfaces are inside the fluid interior, surfaces of both zones should be marked and matched. The yellow surfaces at the Figure 8.5 are interface surfaces of the impeller.

The rotating zone model can also be situated mathematically by defining the relative velocity V_r as:

$$\overrightarrow{V_r} = \vec{V} - \left(\vec{\Omega} x \vec{r}\right) \tag{8.4}$$

where $\vec{r}$ is the position vector in the rotating frame, $\vec{V}$ and $\vec{V}_r$ are actual velocity and relative velocity vectors. By substituting Eq. 8.4 into the general form of the continuity and momentum equations, the new form of those equations based on the relative velocity vector will be obtained. The continuity and momentum equations appear as follows for an inertial reference frame:

$$\vec{\nabla} \cdot \vec{V}_r = 0 \tag{8.5}$$

$$\Delta(\vec{V}_r\vec{V}_r)+(2\vec{\Omega}\times\vec{V}_r+\vec{\Omega}\times\vec{\Omega}\times\vec{r})=-\frac{1}{\rho}\vec{\nabla}\bar{p}+\nabla\left[(\nu+\nu_t)\nabla\vec{\vec{V}}\right] \tag{8.6}$$

As will be mentioned in the further chapters, the turbulence equations also take the new form due to the relative velocity, and became as

$$\frac{\partial\rho k}{\partial t}+\vec{\nabla}.(\rho\vec{\vec{V}}_r k)=\vec{\nabla}.((\mu+\frac{\mu_t}{\sigma_k})\vec{\nabla}k)+p_k-\rho \tag{8.7}$$

$$\frac{\partial\rho\varepsilon}{\partial t}+\vec{\nabla}.(\rho\vec{\vec{V}}_r\varepsilon)=\vec{\nabla}.((\mu+\frac{\mu_t}{\sigma_\varepsilon})\vec{\nabla}\varepsilon)+\frac{\varepsilon}{k}(C_{\varepsilon1}p_k-C_{\varepsilon2}\rho\varepsilon) \tag{8.8}$$

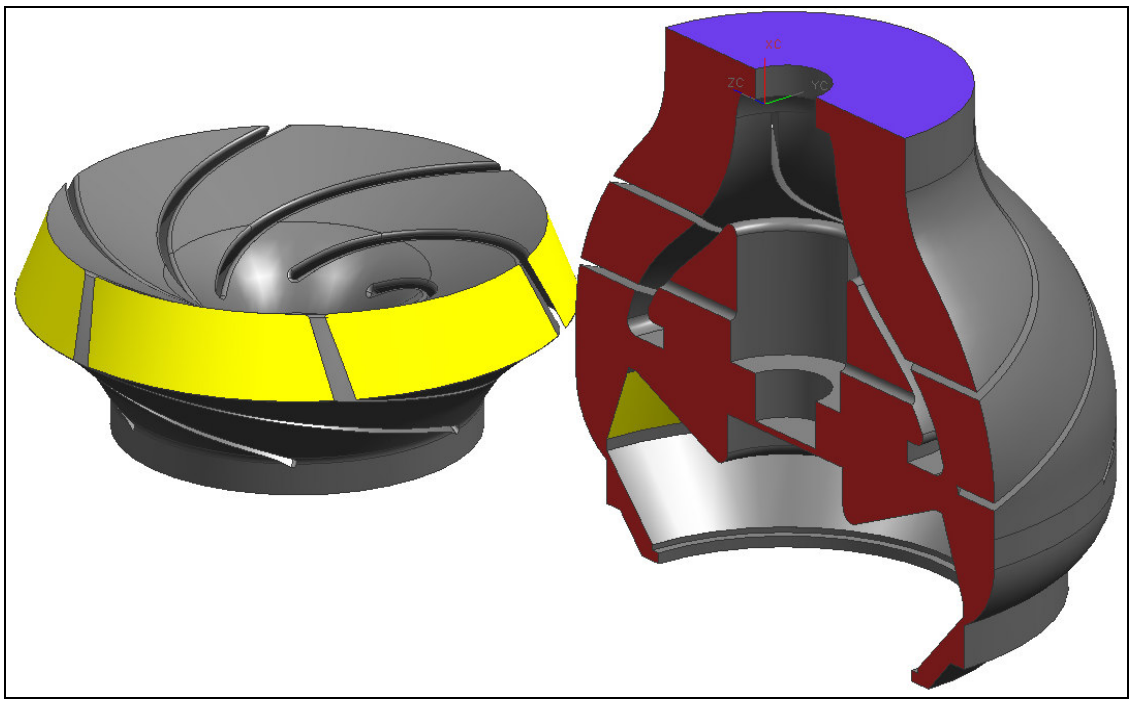

Figure 8.5 – The computational fluid domain inside the diffuser and the impeller.

Therefore, if the equations of motion are revised due to the rotating frame of reference, the acceleration of the fluid should be augmented by the additional terms that appear in the momentum equations. One of the mentioned terms is the centrifugal force and the other one is known as the Coriolis force term in turbomachinery that is

$$\rho(2\vec{\Omega}\times\vec{V}_r) \tag{8.9}$$

8.4.1. The Coriolis Force

When a fluid filled impeller is started to rotate about its axes, due to the centrifugal forces, the fluid gets out from the surface B of the Figure 8.6 that is a semi axial impeller. Therefore, the fluid sucked from the surface E is pressured from the surface B. As indicated in Figure 8.6, a fluid particle inside the impeller will rotate with the impeller at the velocity

$$\vec{V}_p = \Omega.\vec{r} \tag{8.10}$$

about its rotating axis, and at the same time it will move with a velocity W, relative to the impeller, and leave the impeller. U is called the slip velocity, and the W is called the relative velocity (Edis, 1998).

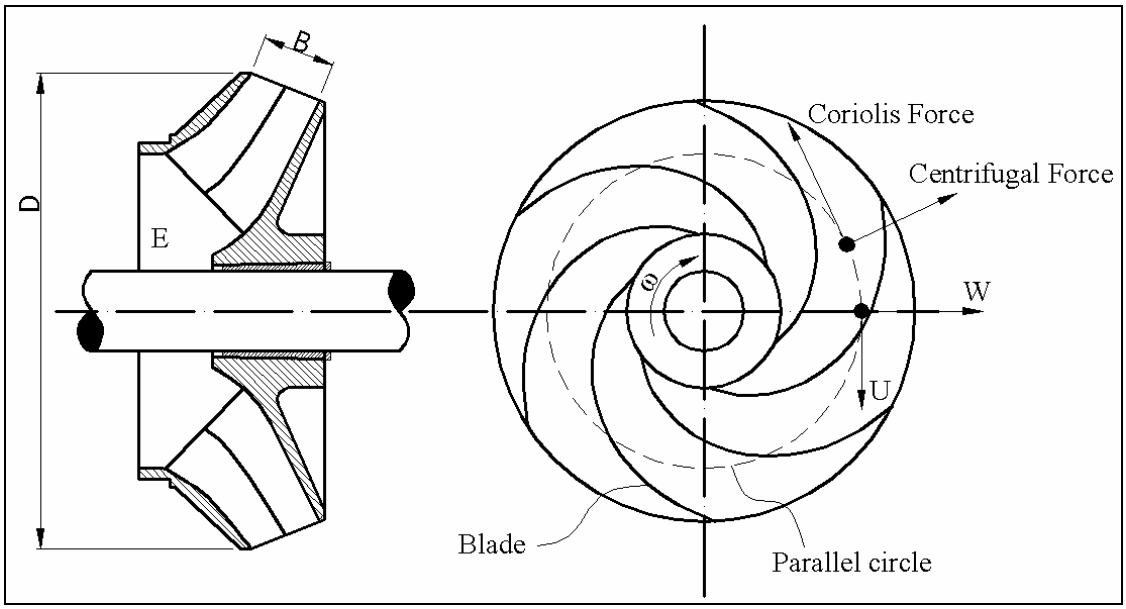

Figure 8.6 – The Coriolis and centrifugal forces acting on a rotating fluid particle.

Since the fluid particle is leaving the axis, the slip velocity is constantly increasing. The difference of the velocity constitutes an acceleration, which is known as Coriolis Acceleration.

As known from the fluid mechanics that, the pressure of a fluid particle will increase in the direction of the applied body forces. Due to the direction of the

centrifugal forces, as the distance from the rotation axis increase, the pressure inside the impeller will also increases. Therefore, the flow will enter from the surface E, and moves trough the blades, and leaves from the surface B. Therefore, the flow will gain pressure while it is passing inside the impeller.

The circles have concentric rotation axis with an impeller are called parallel circles. It can be seen from the Figure 8.6 that the Coriolis forces are tangent to those parallel circles. Therefore, during a motion on those parallel circles in the reverse direction to the rotation, the increase of pressure increase will be noticed due to the Coriolis forces. Therefore, for each parallel circle, the pressure in front of a blade is greater than the pressure behind the blade. Such a pressure distribution causes a negative force in the reverse direction of rotation. These forces, called blade loading, constitutes a negative moment on the rotation axis, in the reverse direction. In order to rotate the impeller, this moment has to be provided at the pump shaft.

8.5. Modeling Wall Roughness Effects in Turbulent Wall Bounded Flows

No slip condition indicates that the fluid sticks to the wall and its relative velocity with respect to the wall is zero (if the wall is moving, fluid on the wall has the same wall velocity). Fluid flows over rough surfaces are encountered in diverse situations. The roughness of the wall has important affect on the velocity distribution in the sublayer and transition regions. Wall roughness affects drag (resistance) and mass transfer on the walls. For the surfaces, which roughness requires to be considered, low of the wall is applied. This theory is used to include the roughness of the surfaces.

The mean velocity distribution near rough walls, has the same slope $(1/\kappa)$ with the smooth ones but with a different intercept (additive constant B in the log-law). The law-of-the-wall for mean velocity modified for roughness has the form

$$\frac{u_p u^*}{\tau_w/\rho} = \frac{1}{\kappa}\ln\left(E\frac{\rho u^* y_p}{\mu}\right) - \Delta B \tag{8.11}$$

$$u^* = C_\mu^{1/4} k^{1/2} \tag{8.12}$$

$$\Delta B = \frac{1}{\kappa} \ln f_r \tag{8.13}$$

and f_r is a roughness function that quantifies the shift of the intercept due to roughness effects.

CHAPTER 9

MESH GENERATION

9.1. Introduction

The governing equations used in the solutions are nonlinear partial differential equations and they can not be solved analytically. In order to solve them numerically over a certain geometry, the domain has to be divided into finite number of subdomains (i.e. finite volumes or finite areas). The governing equations are then solved for each of these volumes under acceptable approximations. The variables are calculated at these discrete locations, which are also called the numerical grid.

In the present study, the numerical grid is generated by the commercial software Gambit. Further information can be found in the Gambit Users Guide. The Gambit software can generate 3D meshes, as in Figure 9.1.

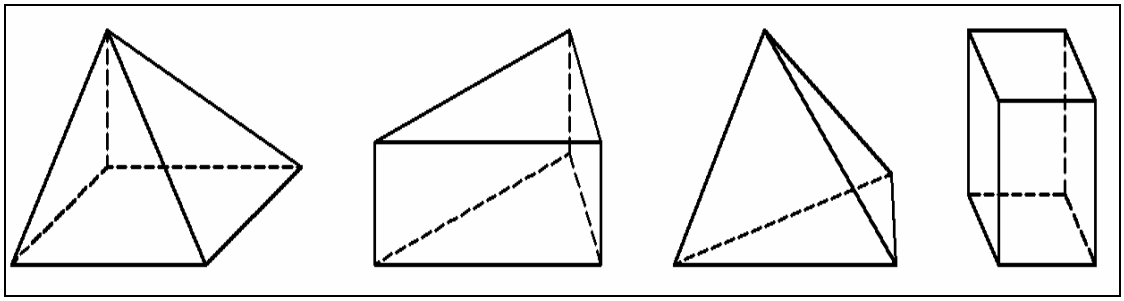

Figure 9.1. Prism, wedge, tetrahedron, and hexahedron type meshes.

9.2. Structured Grid

Regular or structure grids consist of families of grid lines with the property that members of a single family do not cross each other and cross each member of the other families only once. This is the simplest grid structure since it is logically equivalent to a Cartesian grid. The neighbor connectivity of the structured grids simplifies programming and the matrix of the algebraic equation system has a regular structure, which also can be exploited in developing a solution technique.

9.3. Unstructured Grids

For very complex geometries, the most flexible type of grid is one, which can fit an arbitrary solution domain boundary. In principle, such grids could be used for any type of discretization scheme, but they are best adapted to finite volume and finite element approaches. Furthermore, the matrix of the algebraic equation system no longer has regular, diagonal structure; the bandwidth needs to be reduced by reordering of the points. Thus, the solvers of the algebraic equation systems are usually slower than those for regular grids.

It is obvious that more accurate results can be obtained by increasing number of the elements in the mesh. However, this causes increase of computational costs in terms of computation time and the memory requirements. The generated mesh should also completely represent the details of the geometry. Therefore, an optimum number of elements must be considered based on the employed computer capacity. Nevertheless, some methods are developed to obtain accurate results with relatively less number of meshes. In the regions where the flow gradient is high, fine meshes should be employed in order to determine the gradient effects, however for uniform or relatively low gradient regions, rough meshes can be applied. It is obvious that, the domain mesh strategy should be developed based on the problem.

The non–uniform grids can be arranged by a method called size function. In the size function method, the size of the smallest mesh element, size increment ratio, and the maximum required size should be defined. The edges, surfaces or volumes, for which the method applied onto, should also be known. Since it highly affects the number of grids, the increment ratio has to be selected appropriately.

High velocities and surface roughness increase the importance of the boundary layer concept. In order to calculate the shear stresses and the turbulence on a wall correctly, the mesh size of boundary layer region must be sufficiently fine and, the meshes should be aligned with the flow.

The quality of the mesh plays a significant role in the accuracy and stability of the numerical computation. The attributes associated with mesh quality can be listed as node point distribution, smoothness, and skewness. Increasing quality for a mesh will decrease the residuals of the analysis. The generation of a high quality and convenient mesh requires experience and ability of the CFD users.

9.4. Adaption

Mesh is the numerical presentation of the flow geometry. For accurate analysis, the used mesh must have a fine resolution. However, this resolution is restricted by the available computer sources and the required resolution can not be obtained all the time.

The unstructured meshing provides using different mesh sizes for complex geometries. The defined size functions can modify the cell dimensions within a specific algorithm. Therefore, while meshing a complex shape, for the surfaces where the gradient is high, smaller volumes can defined. This method defines the surfaces and the boundary layer effect correctly.

However, the gradients of the flow can be apart from the specified surfaces. In such a situation, the mesh quality will be insufficient to solve the flow for this region. In addition, the exact locations can not be determined unless any - even a poor solution - is obtained. This orients the user to modify the mesh with respect to the results of any obtained solution.

The solution adaptive refinement is defined as the increase of the cells where they are required in the mesh. When the adaption is made properly, the obtained mesh is optimal for the flow solution. This also disables use of extra computer resources. The effect of the mesh refinement on the solution can be studied without completely regenerating the mesh.

The adaption feature works properly within the following conditions:

1- The surface mesh must be fine enough to adequately represent the important features of the geometry

2- The initial mesh should contain sufficient cells to capture the essential features of the flow field

3- A reasonably well converged solution before performing an adaption must be obtained. If an incorrect solution is adapted, cells will be added in the wrong region of the flow.

4- Suitable variables should be selected for performing gradient adaption.

5- Over refining a particular region of the solution domain also causes very large gradients in cell volume. Such poor adaption will affect the accuracy of the solution in the bad way.

Furthermore, for some analysis, the adaption process can be made automatically between a certain numbers of iterations. This type of adaption is called dynamic adaption and useless for the considered problem.

9.5. The Generated Mesh of the Present Study

The mesh generated for the selected problem is based on the triangular element structure as defined before. The employed grids are also non-uniform. Size functions, enable fine grids, are employed around blades of both impeller and diffuser and also for the regions where small geometric details have to be identified, like in Figures 9.2 and 9.3. Another size function is defined for the inlet and the outlet surfaces of the domain (inlet of the impeller and discharge of the diffuser). Since the flow between the diffuser and the impeller is also important, a size function is also applied to these interface surfaces.

It is obvious that the flow is highly turbulent at the tip of the blades. Therefore, these parts should have the smallest meshes. These blades of both diffuser and impeller are covered by boundary layers as seen at Figures 9.4 and Figure 9.5. The boundary layer at these regions keeps its continuity and represents the geometry successfully. The wedge shaped elements aligned with the flow are defined at these regions. This boundary layer has a 0.5 mm meshes at its first row and constantly increases its size with a factor of 1.1. It consist of 4 layers of wedge meshes, and with the given growth factor, this means 2.32 mm of thickness. However, the important part is that this thickness is not the calculated boundary layer thickness: it is estimated to be larger than the real boundary layer thickness.

The problem can be solved for different number of grids. Based on the obtained results, it is observed that 1.000.000 – 1.800.000 meshes are sufficient for reasonable solutions. The mesh used here has 1.576.422 finite volumes.

The used size functions enables the minimum and maximum grids lengths between 1 mm and 8 mm, and the increment ratio is changed from 1.2 to 1.4 based on the region. The values of the applied size functions are listed in Table 9.1

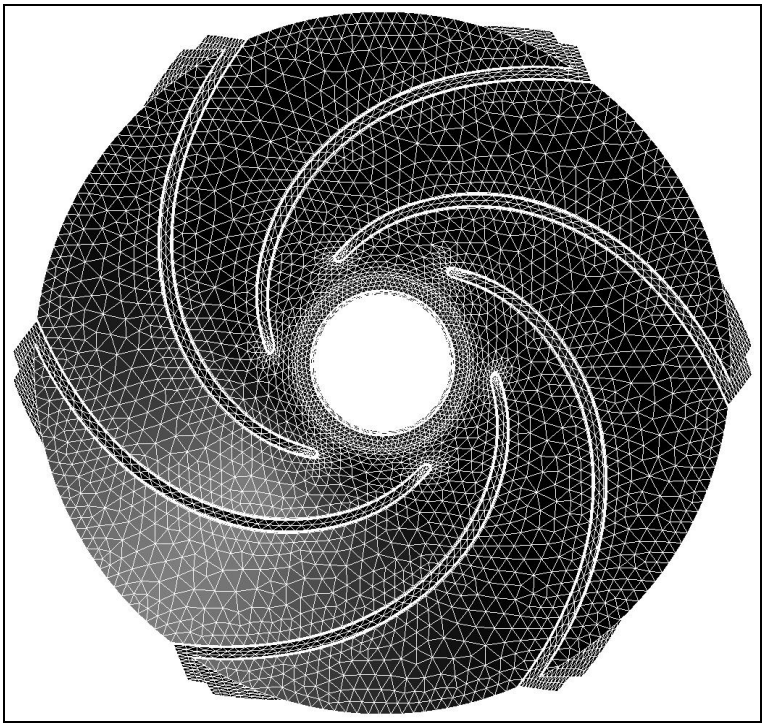

Figure 9.2. Top view of the impeller mesh.

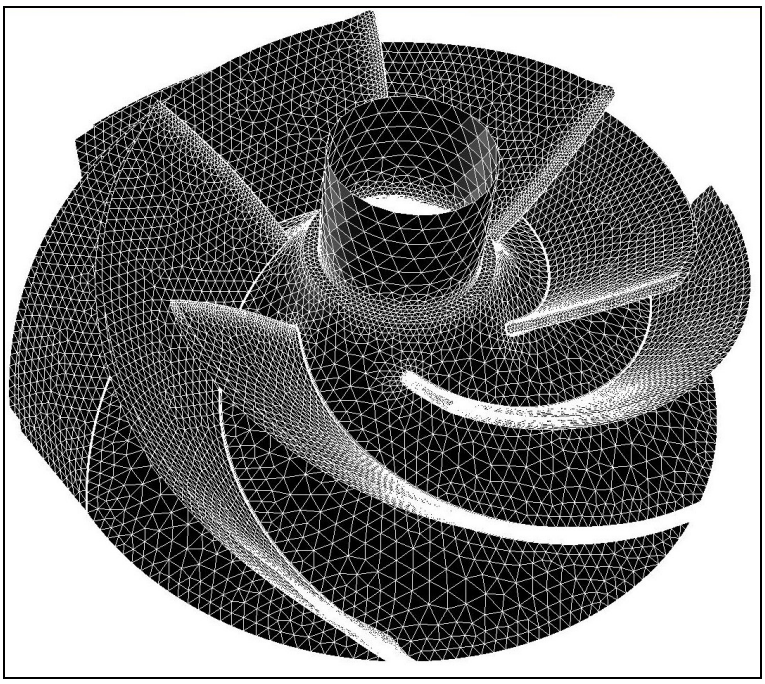

Figure 9.3. The generated mesh for the impeller (the shroud is hided for better view).

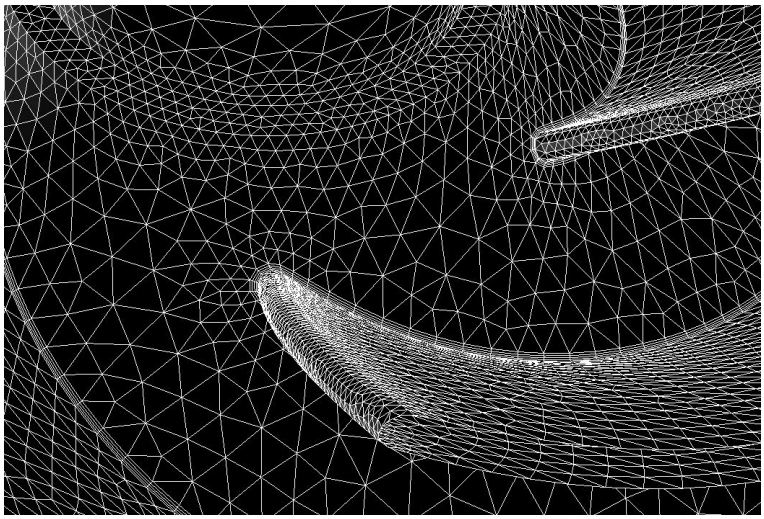

Figure 9.4. The size functions builds fine meshes near the vane and blade tips.

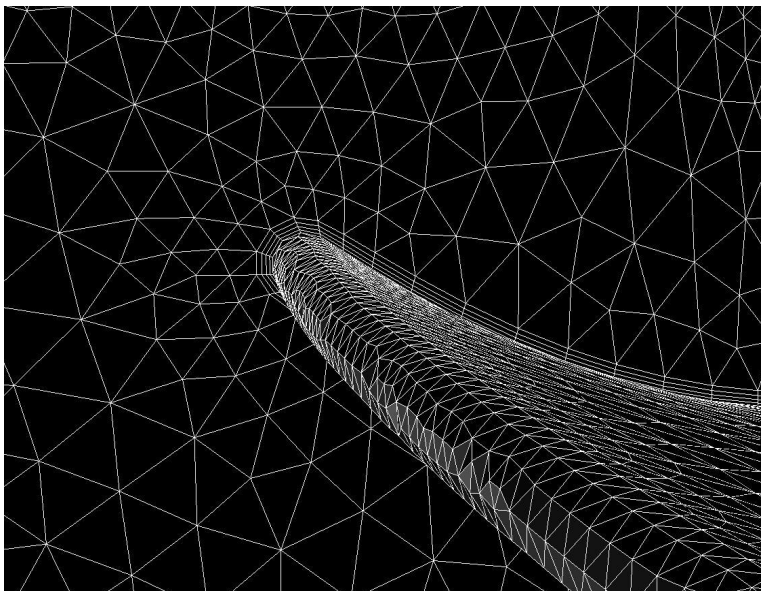

Figure 9.5. Detailed view of the boundary layer defined at the blade surfaces.

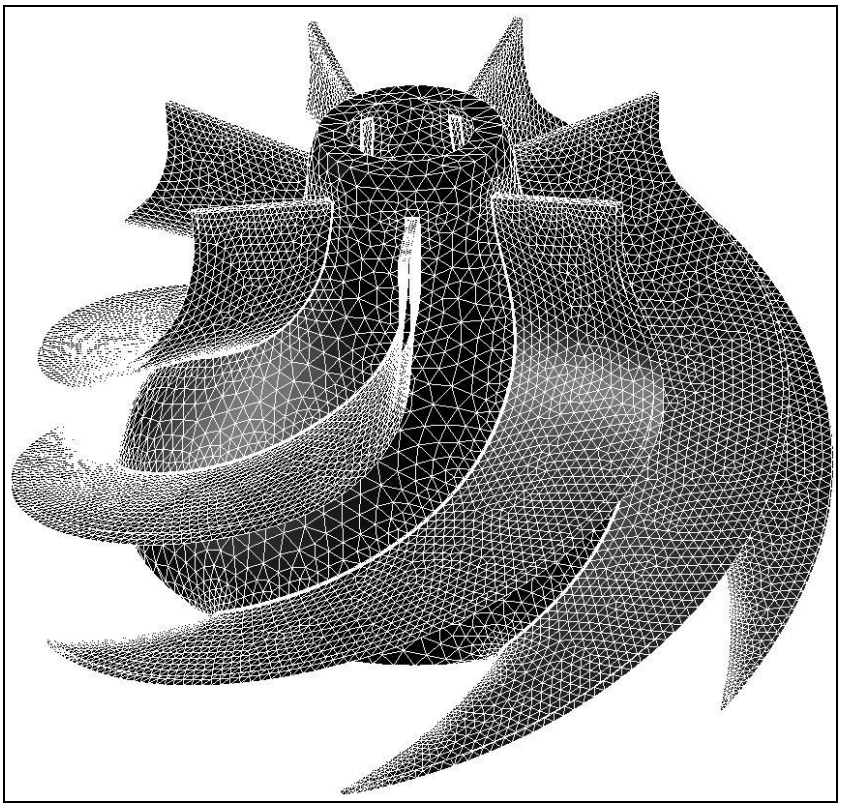

Figure 9.6. The mesh structure of the diffuser (the shroud is hided for a better view).

Table 9.1. The size functions applied to the numerical grid.

IMPELLER			
LOCATION	**Start size**	**Growth Rate**	**Size limit**
Tip of the blades	1 mm	1,20	8 mm
Blade surfaces	3 mm	1,20	8 mm
Inlet of the impeller	3 mm	1,30	8 mm
Interfaces of the impeller	3 mm	1,30	8 mm
Shaft of the impeller	4 mm	1,30	8 mm
DIFFUSER			
LOCATION	**Start size**	**Growth Rate**	**Size limit**
Tip of the blades	1 mm	1,30	8 mm
Blade surfaces	4 mm	1,35	8 mm
Interfaces of the diffuser	3 mm	1,35	8 mm
Discharge of the diffuser	3 mm	1,35	8 mm
Hub surfaces	4 mm	1,35	8 mm
Top of the rotor hub	4 mm	1,35	8 mm
End of blades	3 mm	1,35	8 mm

CHAPTER 10

SOLUTION METHOD

10.1. Solution Approximation

There are three common types of solution techniques generally used today in numerical computations: finite difference, finite volume and finite element. These methods differ in how the equations are discretized, and how they are applied to the elements in the flow domain. It is chosen due the type of the problem (steady or unsteady), shape of the domain, the boundary conditions specified in the problem (i.e. rotating wall motion) and the discretization technique.

The finite differences method calculates the variables of the flow equations at discrete points in the domain. These points are defined by the nodes, which are located at the corners of the elements in the mesh. The finite elements method interpolates the variables within the elements. The order of interpolation determines how accurately the method approximates the continuous solutions of the governing equations.

The method of finite volumes is based on the conservation of mass, momentum and energy laws. These conservations are applied for each control volume of computational domain, and then the obtained set of the algebraic equations are solved. More information about the control volume method and application of it to fluid problems can be found various books (Ferziger, 2002 or Lomax, 1999). One of the most important advantages of this method is its application to complex geometries with different grid types (tetrahedral, quadratic and other) by different gridding strategies including structured, unstructured, hybrid, composite, and overlapping grids.

The Fluent program used in this study, uses finite volume (control volume) technique. Detailed information about the program and method are presented in the Fluent Users Guide (Fluent Inc., 2005).

10.2. Solution Method

Fluent software solves fluid problems by control volume method. The primitive forms of the continuity and momentum equations are solved. Fluent offers different solution methods for solving continuity and momentum equations. These methods are described in various CFD textbooks and in Fluent User Guides.

For unsteady flows, methods based on those used for initial value problems. Steady flow problems are usually solved by pseudo – time marching or an equivalent iteration scheme. These methods used successive linearization of the equations and the resulting linear systems are always solved by iterative techniques. The choice of the solver depends on the grid type and the number of nodes involved in each algebraic equation.

The main difficulty of solving primitive form of the momentum and continuity equation is the pressure terms. There is no equation for pressure terms in the governing equations. Additionally, pressure values on the boundaries, especially solid boundaries, are not known. A special treatment should be employed to obtain the pressure field and establish a relation between velocity and pressure. The pressure values at the surfaces can be interpolated from the momentum equation coefficient if there are not high-pressure variations between the surfaces, thus a smooth distribution is obtained. However, for the flows as in a turbomachine, these conditions can not be meaningful. Instead, a relation between the velocity and pressure must be first obtained from the discrete continuity equation, and then the momentum equations are solved. Some general pressure velocity coupling algorithms can be listed as SIMPLE, SIMPLEC, SIMPLER and PISO.

The acronym SIMPLE stands for Semi Implicit Method for Pressure Linked Equations. The algorithm was originally put forward by Patankar and Spalding (Versteeg, 1995) and is a guess and correct procedure for the calculation of pressure on the staggered grid arrangement. The SIMPLE algorithm uses a relationship between the velocity and pressure corrections to enforce mass conservation and to obtain pressure field. In the present study, SIMPLE method is mainly used.

The main idea of the PISO algorithm is to move the repeated calculations required by SIMPLE and SIMPLEC inside the solution stage of the pressure correction equations. After one or more additional PISO loops, the corrected velocities satisfy the

continuity and momentum equations more closely. This iterative process is called a momentum correction or "neighbor correction". Despite that, the PISO algorithm increases the iteration time, the number of required iterations for convergence decreases.

The SIMPLEC can obtain a converged solution earlier for the uncomplicated flows such as laminar flows, because its under relaxation factor is generally set to 1.0. But of course, this is not valid for a poor quality mesh. In such cases, in order to use skewness correction schemes or more proper under relaxation factors, the SIMPLE algorithm can be used.

As it was mentioned before, in order to convert the governing equations to algebraic equations that can numerically be solved, a control volume based technique is used. This control volume technique consists of integrating the governing equations that conserve each quantity on a control volume basis. At this technique, the discrete values of the scalars can be appointed at both the cell centers and the cell corners. If the values are stored at the cell centers, the face values required for the convection terms must be interpolated from the cell center values. However, a face has two neighboring cell centers. The derivation of the face value from the quantities in the cell upstream or "upwind" relative to the direction of the normal velocity is called upwinding. There are several schemes for upwinding: first order upwind scheme, power law scheme, QUICK scheme and the second order upwind scheme. Details about these schemes, advantages and disadvantages are also given in CDF textbooks (Versteeg, 2005, Fersiger, 2002). Each type of the method yields the same solution if the grid is very fine. However, some methods are more suitable to some classed of problems than others. The preference is often determined by the attitude of the developer.

If the mesh geometry is constructed parallel to flow, the first order convective discretization can be acceptable. However, in a tetrahedral mesh structure, if the flow is not aligned with the cells, the first order convective discretization increases the numerical discretization error. Thus, more accurate results are obtained by the second order discretization (Fluent Users Manual, 2005). In this study, the second order upwind scheme is used for the treatment of convection terms. In this approach, higher order accuracy is achieved at cell faces through a Taylor series expansion of the cell-centered solution about the cell centroid.

The solution method should have certain properties. These properties can be listed as below:

- Consistency
- Stability
- Convergence
- Conservation
- Boundedness
- Reliability
- Accuracy

10.3. Solution Procedure

10.3.1. Coupled and Segregated Solution Procedure

Fluent software offers two solution procedures for the fluid problems, which are segregated and coupled. In the segregated procedure the governing equations are solved sequentially (i.e., segregated from one another). Since the equations are non-linear (and coupled), several iterations of the solution loop must be performed before a converged solution is obtained. The segregated process method can be outlined as:

1- Fluid properties are updated, based on the current solution (also the initialization of the solution)

2- The momentum equations are solved in turn using the current values for pressure and face mass fluxes, in order to update the velocity field

3- Since the velocities obtained in the previous step may not be satisfy the continuity equation locally, a “Poisson-type” equation for the pressure correction is derived from the continuity equation and the linearized momentum equations. This pressure correction equation is then solved to obtain the necessary correction to the pressure and velocity fields and the face mass fluxes such that continuity is satisfied

4- Where appropriate, equations for scalars such as turbulence, energy, species, and radiation are solved using the previously updated values of the other variables

5- When interphase coupling is to be included, the source terms in the appropriate continuous phase equations may be updated with a discrete phase trajectory calculation

6- A check for convergence of the equation set is made

These steps are repeated until the convergence criteria are met.

The difference of the coupled solver from the segregated solver is that the coupled solver solves the governing equations of continuity and momentum simultaneously. Governing equations for additional scalars like turbulence are solved sequentially using the procedure described for segregated solver. Since the governing equations are non-linear, several iterations of the solution loop must be performed before a converged solution is obtained. In the coupled approach:

1- Fluid properties are updated, based on the current solution. The fluid properties are defined by the initialized solution parameters at the beginning of the solution

2- The governing equations are solved simultaneously

3- Equations for turbulence are solved using the previously updated values of the other variables

4- A check for convergence of the equation set is made.

Both the segregated and coupled procedures will provide results for a broad range of flows, but the convenient procedure should be selected based on the domain and flow conditions. These procedures differ in the way that the continuity and the momentum equations are solved.

In the present study, the implicit segregated procedure is used.

10.3.2. Implicit and Explicit Method

In the finite volume method, the continuity and momentum equations are integrated over each grid and algebraic equations are constructed for each cell. All the variables of cell are influenced from its neighbors and in order to solve them they have to be linearized. Thus, the manner in which these governing equations are linearized may take an “implicit” or “explicit” form.

In the implicit form, a set of equations are constructed from all the existing and unknown variables of all the cells. After an arrangement, there appears same number of equations and unknowns. Thus solving this equation set will provide all the unknowns.

The explicit form is simpler with respect to implicit form. In the explicit form, the unknowns of the each cell are computed by the existing values. Thus all the variables can be calculated easily by their own equation.

The segregated approach solves for a single variable field by considering all cells at the same time. It then solves for the next variable field by again considering all the cells at the same time, and so on. Therefore, there is no explicit solution for the segregated solver. On the other hand, the coupled solution method can use both the forms to calculate the variables.

10.4. Initial Conditions (Initializing)

For many complex flow problems such as those found in rotating machinery, or flows in expanding or spiral ducts, flow convergence can be accelerated if a better initial solution is used at the start of the calculation. This means that if the values for all the cells are close to the actual solution; it will be easy to reach the required solution. The mentioned initial conditions can be provided by iterating the equations by the first order explicit form starting from the inlet boundary (the inlet surface is set to mass flow inlet boundary condition). A few iterations after, the initial conditions are more or less defined for all cells and then the actual solution method can be executed. In this manner, the present study is initialized with 5 first order iterations.

In addition, after obtaining just one converged solution for a case, the other solutions for the same case can be executed by just changing the boundary condition. Thus, result of a solution can be used for the initial condition for another problem. In the present study, after obtaining and saving the solution for a flow rate, the flow inlet boundary condition is set to other required value, and the computer is made to continue iterating.

10.5. Setting the Under Relaxation Factors

The under relaxation factors are used by the segregated solver to control the update of the computed variables at each iteration. For a course mesh or for a high turbulent complex flow, the under relaxations may be decreased. This also causes to make more iteration for convergence.

10.6. Residual Convergence Criteria

The convergence criteria are needed to be set for the iterative methods. Usually, there are two levels of iterations: inner iterations, within which the linear equation are solved, and outer iterations that deal with the nonlinearity and coupling of the equations. Deciding, when to stop the iterative process on each level is important, from both the accuracy and efficiency points of view.

Residuals are defined as the RMS (root mean square) of the error between two iterations. Theoretically, the residuals will go to zero as the solution converges. However, practically, residuals decrease up a very small value. For the analysis on a high capacity computer that can handle double precision, they can reach to 10^{-12} level, and for the single precision solutions, 10^{-6} level residuals can be reached.

10.7. Employed Computer and Computational Time

The computer used for the analysis is desktop personal computer with Intel Pentium 4 – 3.0 Prescott processor and it has 2 GB of RAM. The processor and the main board have Hyper-Threading Technology, which enables to use computer during iterations. This amount of RAM can handle 1,8 million meshes.

CHAPTER 11

RESULTS AND DISCUSSIONS

The centrifugal pumps, governing equations of the flow inside a pump and numerical solution methods in order to obtain velocity and pressure distributions were introduced in previous chapters. The pump for which the analyses are made were also described. Boundary condition types were also explained in details.

The selected pump VDP 1433 has a specific constant geometry. The capacity, head and the consumed power of the pump has been determined by a calibrated and high-resolution test stand (Değer, 2004). The working conditions of the pump are also defined by the Vansan Company already (i.e. density and max temperature of the fluid, rotational speed, etc.).

As it was mentioned before, the aim of this study is to solve the governing equations of the flow inside the selected pump. Thus, the prior results of the problem will be the velocity and pressure distributions. Additionally, these results enable solver to determine the consumed power, the head of the pump and consequently its efficiency.

The design point of the pump, also the experimental best efficiency point, is found at 120 kg/s. Thus, the main detailed study for visualization of flow patterns and pressure distribution are performed for the best efficiency point. Although the pump should work at best efficiency point, the pressure and the velocity distributions for 90 kg/s to 150 kg/s with 10 kg/s interval are also obtained and investigated.

The generated mesh with 1576422 number of elements and 2.32 mm thick boundary layer is used within the analysis. To model the turbulence, standard $k-\varepsilon$ model is selected. Since the flow inside the pump is turbulent, the roughness of the solid surfaces may affect the flow. The variation of pressure and velocity with respect to roughness is another part of the present work. The rotational speed of the impeller fluid domain is set to 1450 rpm. For the inlet surface, mass flow inlet boundary condition, and for the outlet, a constant static pressure of 500 kPa is defined. This defined static pressure is greater than the expected total pressure of the pump. The pressure at the inlet is calculated from the interior of the domain and different for each analysis.

11.1. Ideal Pressure and Velocity Distributions

Before starting to explain the results of the study, it might be useful to mention about the ideal velocity and pressure distributions inside a pump. The aim of a pump designer is to design the pump close to its ideal conditions. Therefore, the ideal hydrodynamic behaviors of both impeller and diffuser should be known.

For the impeller, firstly, the region between the blades should be inspected. At its ideal condition, the static pressure should increase from the entrance of the blade to the outlet steadily and uniformly. No disturbances in pressure and velocity are desired. The streamlines that are started near the inlet region should follow a smooth path. The velocity vectors should be parallel to the flow and no swinging, rotation, spin, screw or direction change should occur. The dynamic pressure for the impeller should increase steadily with the increase of magnitude of velocity vectors. The velocity vectors at the entrance region should be at the normal to the inlet surface.

For the diffuser, the dynamic pressure should steadily decrease from inlet to the discharge. There should not be any back flows or vortex paths. The total pressure contours should be smoothly increasing on the hub surface.

The flow pattern between the impeller and the diffuser fluid zones should also be evaluated. The motion of fluid from impeller to the diffuser, the flow at the interface surfaces should also be smooth. The flow should not be separate from the back surfaces of the impeller and diffuser blades.

The results of analysis for different flow rates should be used to obtain the characteristic curve of the pump. The obtained characteristic curve should also be compared with the experimental results. Apart from the values of the results, the match of the curves should be evaluated. The determination of the head capacity curve is more important and should be initially evaluated. Then the power capacity curve should be matched with the experimentally measured one. If these two curves perfectly match, the efficiency curve has to match.

It should be noted that, during the comparison of the curves, there can be fixed differences between the experimental and numerical curves. Even one of the curves look like the offset or shifted of the other curve. This situations show that these numerical analysis can also represent the experimental data, but there still exists a numerical error.

11.2. The Employed Physical and Computational Constants

The governing equations and methods have some coefficients and constants that have to be defined. These constants, which are given below, are used for all runs in the present study;

- The properties of the fluid:

ρ : 998.2 kg/m^3

C_p : 4182 j/kgK

μ : 0.001003 $kg/m-s$

- Constants for turbulence models

C_μ : 0.09

$C_{1\varepsilon}$: 1.44

$C_{2\varepsilon}$: 1.92

σ_k : 1

σ_ε : 1.3

- Constants for convergence

Residual for continuity : 10^{-5}

Residuals for velocity : 10^{-6}

Residual for k : 10^{-5}

Residual for ε : 10^{-5}

- Constants for under relaxation factors

Pressure : 0.3

Density : 1

Momentum : 0.7

Turbulence kinetic energy : 0.8

Turbulence dissipation rate : 0.8

Turbulent viscosity : 1

11.3. Methods of Comparison between Obtained Results

One of the most important parts of the evaluation of obtained results is the post processing part. To compare the obtained results the velocity and pressure distribution have to be plotted and visualized, however the positions and the colors and the data labels have to be same for all figures.

In order to compare the obtained results with an ideal pump, and to compare results of different flow rates with each others and to see the effect of the surface roughness, both for impeller and diffusers, the following distributions are obtained and plotted for both impeller and diffusers:

1- The static, dynamic and total pressure the pressure distributions on the walls of impeller and diffuser blades are calculated and plotted. However, the plotted figures are colorful, so for a better comparison, the ranges of colors corresponding to the range of pressure should be made same for all figures. Therefore, same color ranges are used in all pressure figures. The adjusting of color ranges is especially difficult for the problems with mass flow inlet boundary conditions since the head values between different cases are different and thus the inlet pressure varies. As it was mentioned before, the pressure at the inlet surface is calculated from the interior of the domain. Therefore, the pressure difference between the inlet and the outlet surfaces should be used. Since the static pressure at the outlet is defined and constant for all flow rates of the analysis, the inlet static and dynamic pressure is expected to increase with the increasing flow rate. Actually, the pressure values of the whole domain should be arranged due to the inlet static pressure. Then the selected range for the static pressure, that covers all analysis, should be defined for each analysis. Similarly, for the total pressure, in addition to the static pressure, maximum dynamic pressure should also be considered and the total range should be determined.

2- The velocity vectors in impeller and diffuser are plotted. This also provides the visualization of flow inside the pump. Since the velocity is a vectoral quantity, besides its scalar quantity, the direction of the flow is also plotted. This is provided by the colorful velocity vectors and colors represent the velocity magnitude.

3- Flow patterns inside the impeller and diffuser are also plotted. These patterns show fluid paths. This provides better view for understanding of flow inside the pump.

11.4. Comparison of the Numerical Results with Experimental Results

The numerical analyses are questionable unless they are compared with the experimental results. Also, in order to compare a numerical analysis, the residuals should converge to the desired level. Then numerical results can be compared with the experimental ones, and the differences should be commented. Unfortunately, it is not easy to compare the velocity and pressure distribution between experimental and numerical results. However, the obtained head, consumed power and efficiency of pump for different mass flow rates can be compared with the numerical results. A good agreement between the numerical and experimental curves will sufficiently prove the accuracy of the numerical results.

The calculated head of the pump is the total pressure difference between the outlet and inlet surfaces of the whole domain. Since mass flow boundary condition is defined for the inlet area, the pump capacity is defined already.

The input power of the pump is calculated from the torque on the rotor surfaces. The total of pressure and viscous moments on the blade, hub, shroud surfaces, and also the moment on the shaft and rotor top surfaces will equal to the applied power. The required power for the analyses can be obtained as:

$$P_{INPUT} = n_{pump} \cdot T \cdot \frac{2\pi}{60} \tag{11.1}$$

where P_{INPUT} is the power, n_{pump} is the rotational speed, and T is the torque on the surfaces.

11.5. The First Analysis: Zero Roughness on the Surfaces

The first analysis is made with zero roughness in order to find the effect of roughness in the following analysis. In Figure 11.1, the convergence of residuals for 120 kg/s is represented. The numerical values of the whole analyses are given in Table 11.1. As seen from the table, the maximum calculated efficiency is 83.1% corresponds to the 120 kg/s mass flow rate. If this data is compared with the experimental results on

a chart as it is shown in Figure 11.2, a perfect agreement between the calculated and experimental efficiency can be observed.

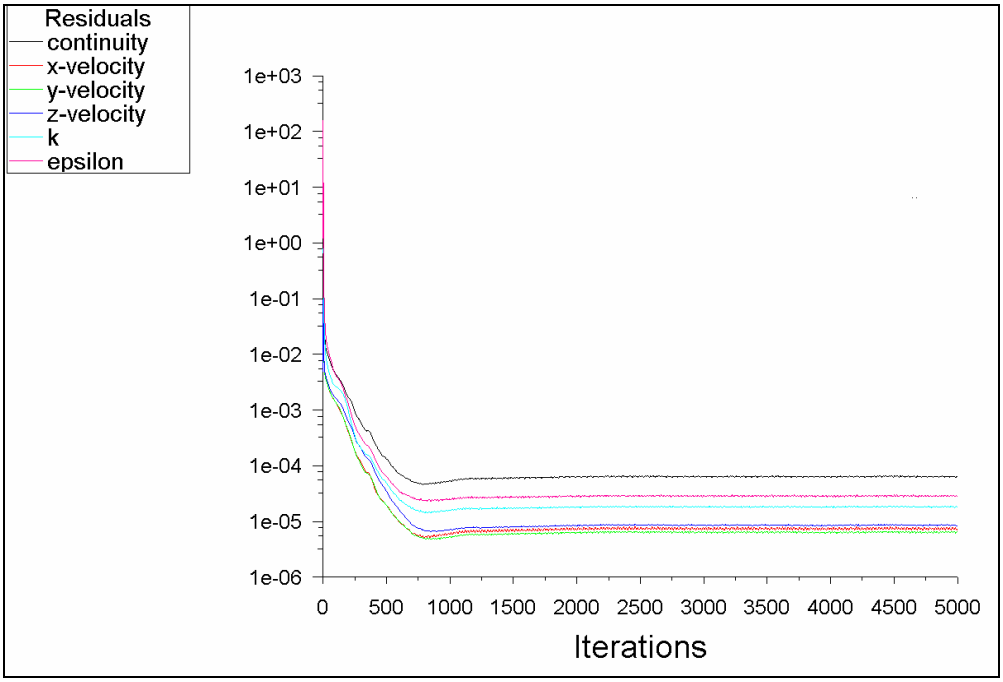

Figure 11.1 The residuals at 120 kg/s with zero roughness on the walls.

Table 11.1 The numerical results for the first analysis with zero roughness on the walls.

Speed	**Torque**	**Power**	**Total Pressure at Outlet**	**Total Pressure at Inlet**	**Total Pressure Difference**	**Flow rate**	**Head**	**Efficiency**
rpm	**Nm**	**kW**	**kPa**	**kPa**	**kPa**	**kg/s**	**Water Column**	**%**
1450	**148.9**	22.6	**515.4**	**317.6**	197.8	**90.0**	20.2	78.9
1450	**153.5**	23.3	**517.0**	**328.0**	188.9	**100.0**	19.3	81.2
1450	**158.2**	24.0	**518.2**	**337.7**	180.5	**110.0**	18.4	82.8
1450	**162.3**	24.6	**519.1**	**348.7**	170.4	**120.0**	17.4	83.1
1450	**165.0**	25.1	**520.4**	**361.9**	158.5	**130.0**	16.2	82.4
1450	**166.1**	25.2	**522.3**	**377.2**	145.1	**140.0**	14.8	80.6
1450	**165.4**	25.1	**523.9**	**393.8**	130.1	**150.0**	13.3	77.8

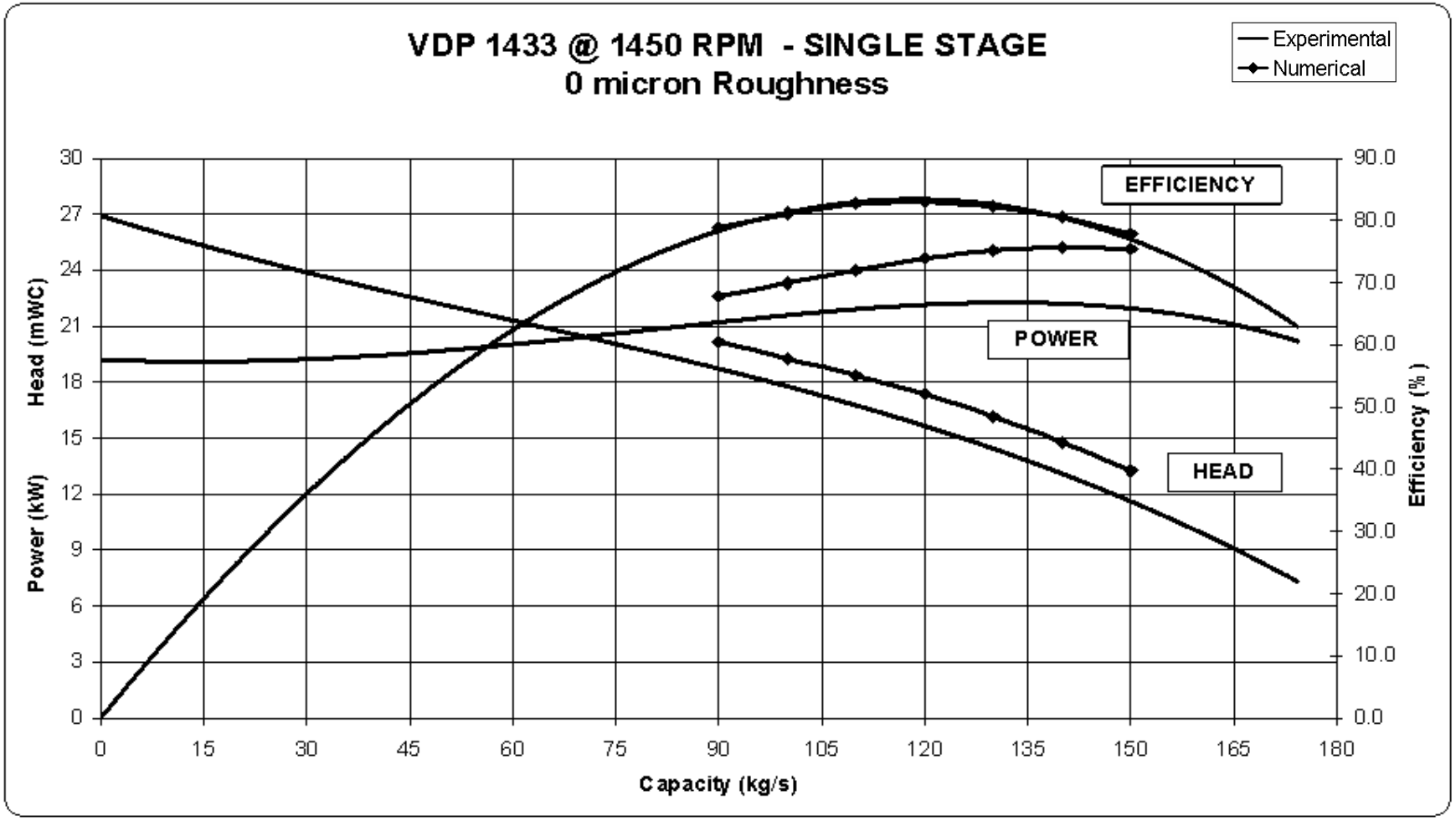

Figure 11.2. The comparison with the experimental results.

The match of the efficiency curves can be misleading because the head and power curves have not such a perfect match. Instead, they both are greater than the experimental values. Their ratio, coincidentally, makes the efficiency curves be matched with each other.Although, there are differences between the head and the power of experimental and numerical results, the trend of the numerical results follow the trend of experimental data. (Figure 11.3) The difference between the actual head is constant and independent of the flow rate. The maximum relative difference between the numerical and the experimental values is 1.72 WC.

On the other hand, the consumed power is also higher and the difference increases with the increasing flow rate. The consumed power is directly related with the pressure and viscosity moments on the surfaces. If these two moments are compared, as in Figure 11.3 for different flow rates, it can be observed that the pressure moment is the dominant to the viscous moment. Since the calculated pressure is higher on the surfaces, the pressure moment is also calculated higher.

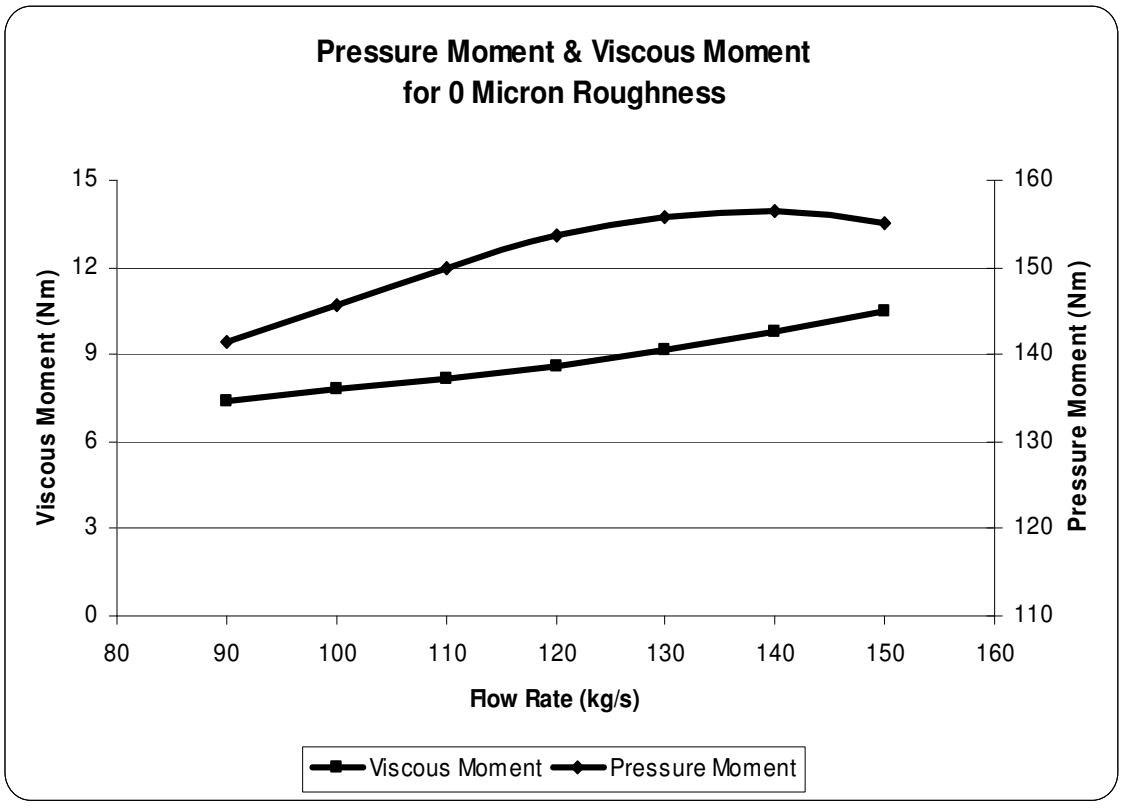

Figure 11.3 The comparison of the pressure and viscous moments with respect to flow rate for zero roughness on the walls.

11.6. Effect of Roughness

In order to consider the effect of the roughness on fluid flow, the wall functions and fine meshes close to the walls are employed since the roughness on the walls has important affects. So far the analyses were made with the zero roughness on the walls.

The considered pump is manufactured by the casting method. After casting, the outer shell of the impeller and some partial of the diffuser are processed by the CNC machines. The unprocessed surfaces, however, have acceptable roughness values even after smoothing and polishing. In order to model this roughness value, and to see its effect, an investigation is performed. Since the used sand in the casting is same for all pumps, the roughness should be the same for all pumps. The surfaces that the roughness must be applied are hub, shroud and blades surfaces of both the impeller and diffuser.

The upper part of the impeller hub, which is included in the analysis is processed by the CNC machines and so no roughness should be applied to this surface.

The surface roughness is measured with sensitive instruments. However, in this study, in order to measure the roughness, the analyses are made with three different values, and the effect of the roughness is investigated. The roughness is represented by two values in the analysis: the roughness value and the roughness constant. The roughness constant is assumed to be the same for all analysis and is accepted as 0.5.

The results of the analysis with different roughness values are compared with the experimental results below in Figure 11.4, 11.5, 11.6. As can be noticed, increase in roughness slightly affects the consumed power. However, the main effect of the increasing roughness is on the total head. As the roughness increases, the calculated total head decreases.

From the pump curves, presented in Figures 11.3, 11.4, 11.5, 11.6, the best one that has a good agreement with experimental results is found to be the Figure 11.4, in which the surfaces have 50-micron roughness. The 50-micron roughness value makes the numerical efficiency curve has the same curvature with the experimental efficiency curve, and at the same time, has the closest head capacity curve among the other values.

Table 11.2. Numerical values of the analysis with 50-micron roughness on the walls.

50 micron								
Speed	**Torque**	**Power**	**Total Pressure at Outlet**	**Total Pressure at Inlet**	**Total Pressure Difference**	**Flow rate**	**Head**	**Efficiency**
rpm	**Nm**	**kW**	**kPa**	**kPa**	**kPa**	**kg/s**	**Water Column**	**%**
1450	**149.1**	22.6	**514.7**	**318.6**	196.2	**90.0**	20.0	78.0
1450	**153.7**	23.3	**516.7**	**329.2**	187.4	**100.0**	19.1	80.3
1450	**158.5**	24.1	**517.9**	**339.0**	178.9	**110.0**	18.2	81.7
1450	**162.6**	24.7	**518.7**	**350.1**	168.6	**120.0**	17.2	81.9
1450	**165.3**	25.1	**520.1**	**363.6**	156.6	**130.0**	16.0	81.1
1450	**166.3**	25.3	**522.1**	**379.3**	142.8	**140.0**	14.6	79.1
1450	**165.6**	25.1	**524.0**	**396.7**	127.3	**150.0**	13.0	75.9

Table 11.3. Numerical values of the analysis with 100-micron roughness on the walls.

100 micron								
Speed	**Torque**	**Power**	**Total Pressure outlet**	**Total Pressure inlet**	**Total Pressure Difference**	**Flow rate**	**Head**	**Efficiency**
rpm	**Nm**	**kW**	**kPa**	**kPa**	**kPa**	**kg/s**	**Water Column**	**%**
1450	**151.1**	22.9	**514.5**	**321.5**	193.0	**90.0**	19.7	75.6
1450	**155.3**	23.6	**516.5**	**333.4**	183.1	**100.0**	18.7	77.6
1450	**159.6**	24.2	**517.9**	**344.5**	173.4	**110.0**	17.7	78.7
1450	**163.2**	24.8	**519.3**	**357.6**	161.6	**120.0**	16.5	78.3
1450	**165.5**	25.1	**521.6**	**373.4**	148.2	**130.0**	15.1	76.6
1450	**166.3**	25.2	**523.6**	**390.6**	133.0	**140.0**	13.6	73.7
1450	**165.6**	25.1	**526.2**	**410.2**	116.1	**150.0**	11.8	69.2

Table 11.4. Numerical values of the analysis with 250-micron roughness on the walls.

250 micron								
Speed	**Torque**	**Power**	**Total Pressure outlet**	**Total Pressure inlet**	**Total Pressure Difference**	**Flow rate**	**Head**	**Efficiency**
rpm	**Nm**	**kW**	**kPa**	**kPa**	**kPa**	**kg/s**	**Water Column**	**%**
1450	**151.4**	23.0	**514.0**	**323.0**	191.0	**90.0**	19.5	74.7
1450	**155.7**	23.6	**516.0**	**334.7**	181.3	**100.0**	18.5	76.6
1450	**159.9**	24.3	**517.2**	**346.0**	171.2	**110.0**	17.5	77.5
1450	**163.5**	24.8	**518.7**	**359.5**	159.1	**120.0**	16.2	76.9
1450	**165.7**	25.2	**520.9**	**375.7**	145.2	**130.0**	14.8	75.0
1450	**166.4**	25.3	**523.2**	**393.3**	129.8	**140.0**	13.2	71.9
1450	**165.6**	25.1	**525.8**	**413.2**	112.6	**150.0**	11.5	67.1

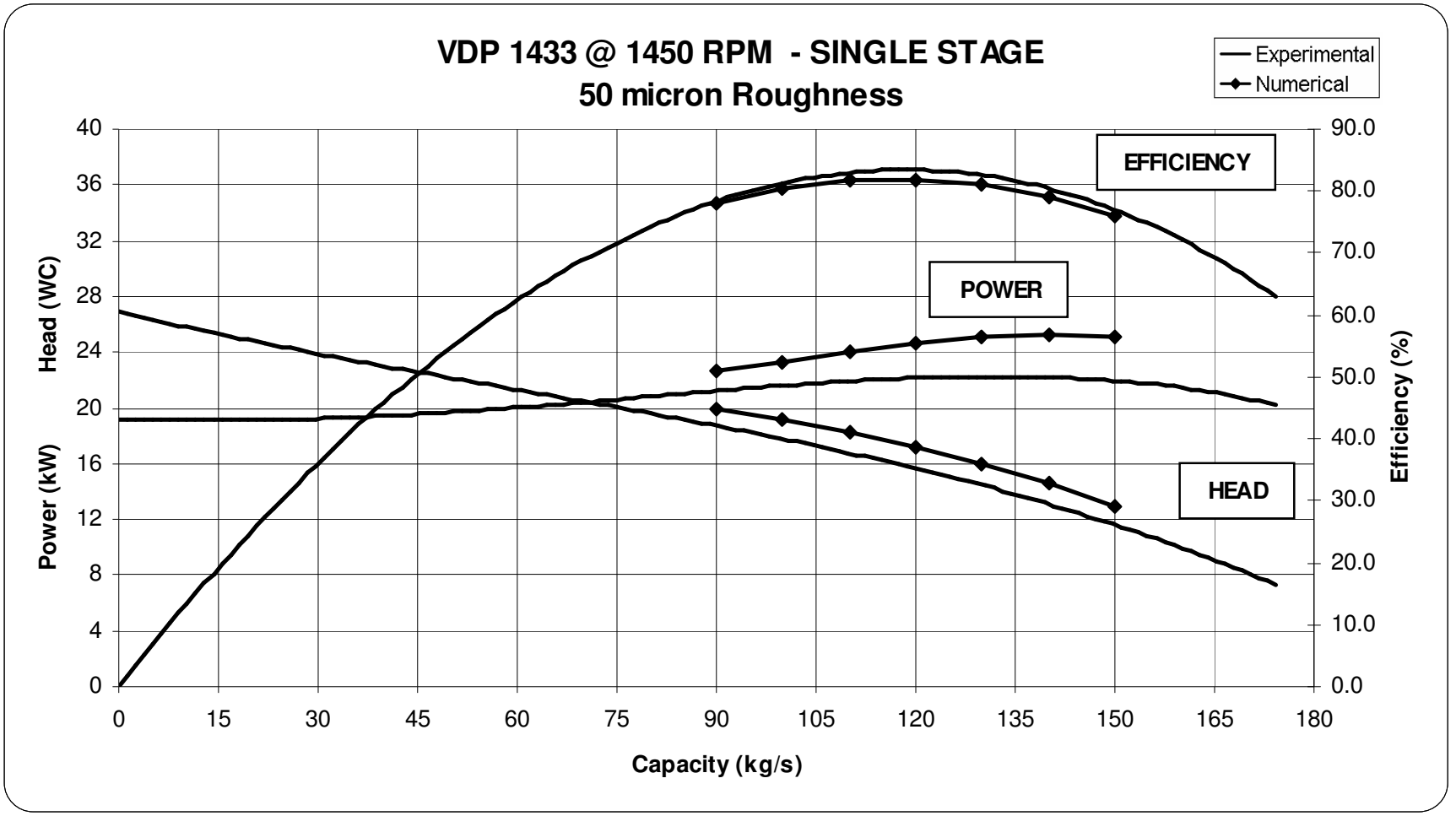

Figure 11.4. The comparison of the 50-micron roughness with the experimental results.

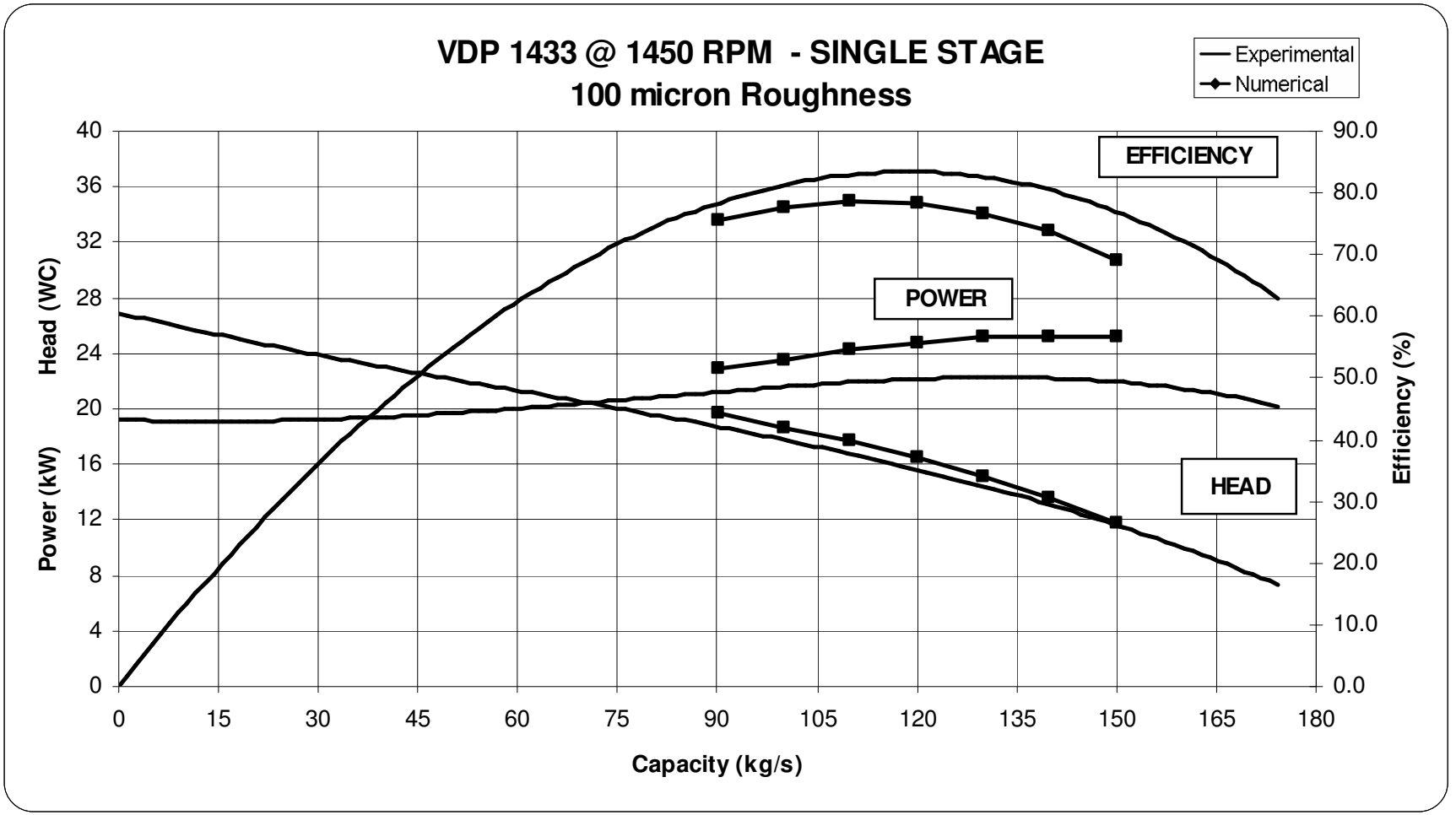

Figure 11.5. The comparison of the 100-micron roughness with the experimental results.

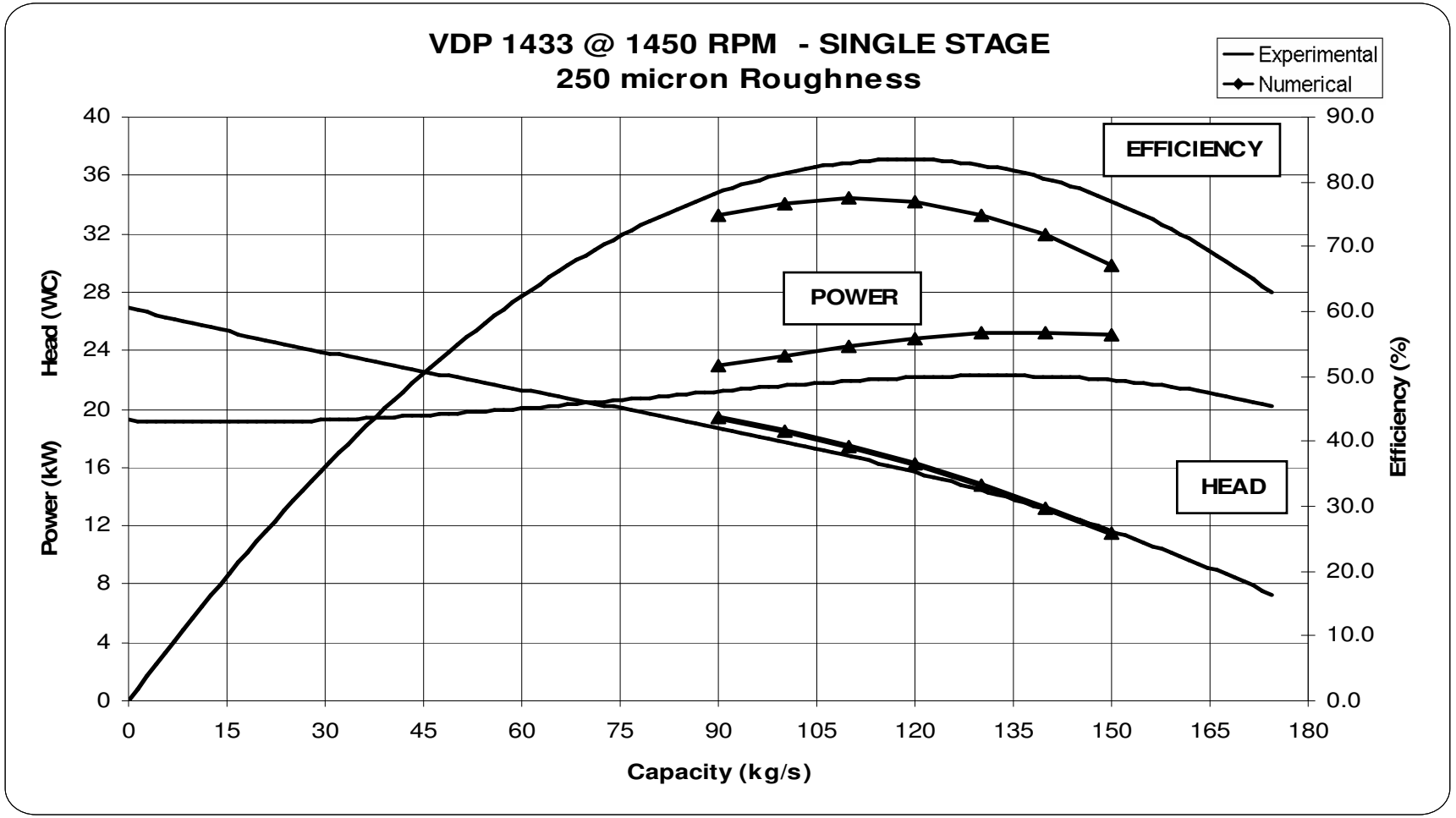

Figure 11.6. The comparison with the 250-micron roughness with the experimental results.

11.6.1. Effect of Roughness on Consumed Power

The analysis shows that the head is more sensitive to roughness rather than the consumed power, and it seems the consumed power is slightly affected from the roughness. In this section, it is struggled to explain this different behavior between head and consumed power.

There is no doubt that by increasing the surface roughness, turbulences on the surfaces occur and friction increases. Thus a part of power, which is imposed to the fluid, is consumed to overcome the friction. This causes the pump head to decrease. By increasing the roughness, the friction increases and consequently the head decreases more.

However, the same trend is not observed for power. As mentioned before, power is calculated from the rotation speed and moment on the impeller surfaces. The moment on the impeller surfaces has two components; the pressure moment and the viscous moment. This means that two types of forces are applied onto the surfaces of impeller, one related to pressure force and the other one is the shearing forces due to both kinematic and Reynolds stresses. To visualize the change of these momentum components, they have been compared with the values of zero roughness analysis in Figures 11.7, 11.8, 11.9. As seen from the figures, with the increasing roughness, the pressure moment decreases while the viscous moment increases. These figures show that, increasing the surface roughness increases the viscous moments. This is an expected result, since the friction due to roughness increases. Besides this, the pressure moment also decreases since the head of the pump decreases. The increase in power due to viscous moment is compensated by the decrease in the pressure moment. That is why the increase of the roughness does not affect the consumed power. Since the geometry is large, and the power is mainly dominated by the pressure moment, the effect of roughness on the viscous moment is negligible. However, if a smaller domain is considered, for example, if a 6” pump was analyzed instead of a 14” pump, the effectiveness of the viscous moment will increase. Thus in such a situation, roughness value of the surfaces has more effect on the consumed power, and will increase the consumed power for small pumps.

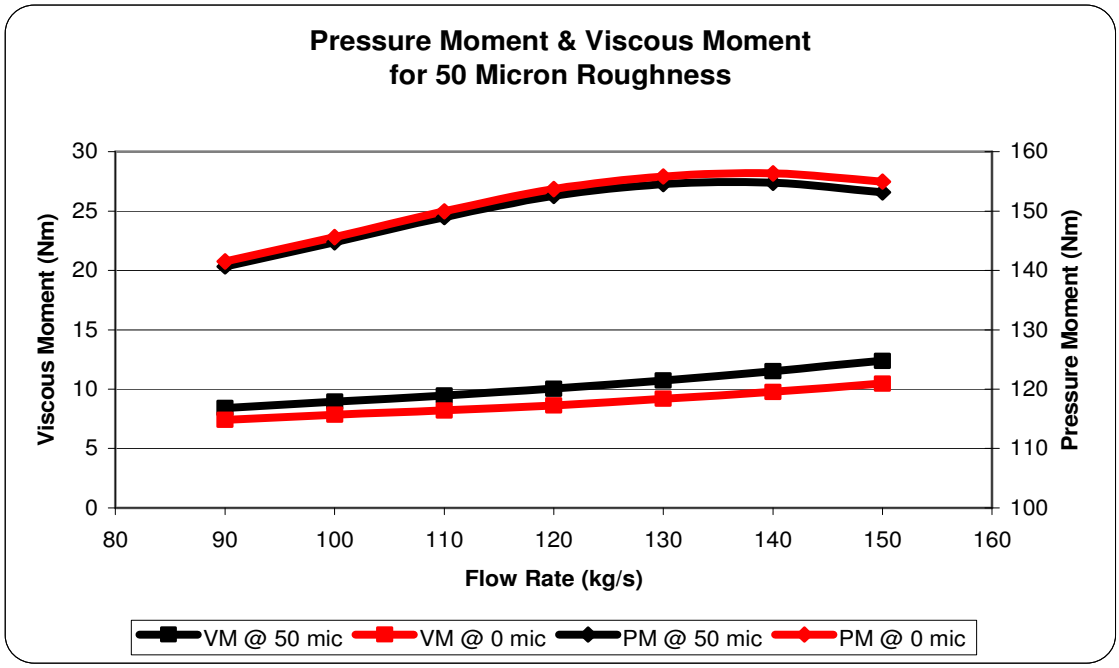

Figure 11.7. The comparison of the 50-micron roughness with zero roughness.

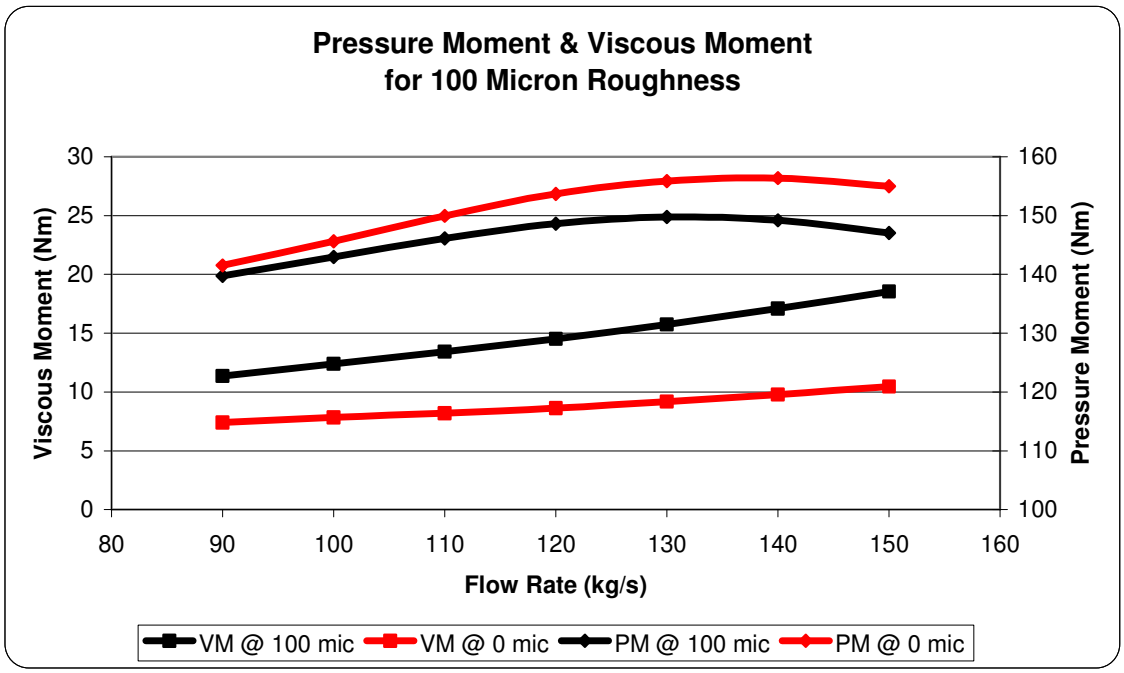

Figure 11.8. The comparison of the 100-micron roughness with zero roughness.

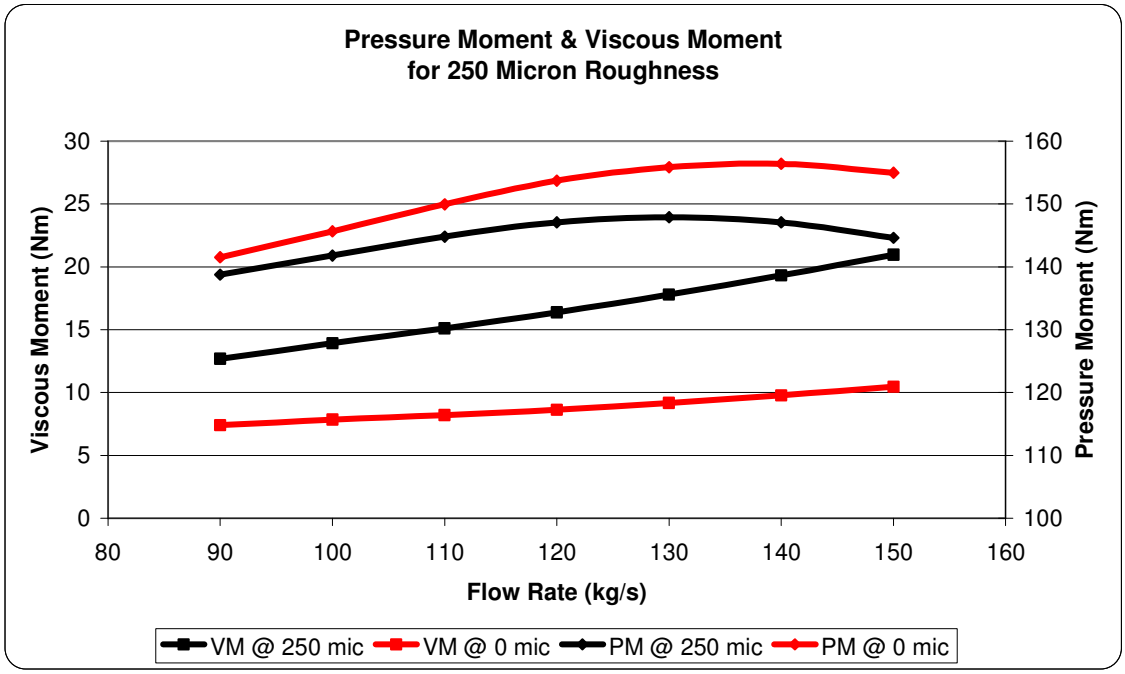

Figure 11.9. The comparison of the 250-micron roughness with zero roughness one.

11.7. Pressure Distribution Inside the Pump at BEP

Pumps are designed for a specific flow rate. All the angles and profiles are determined for a working point. For the improvement of a pump design, the analysis should be performed at the best efficiency point. In this section, the variation of pressure in the pump section, containing the impeller and diffuser is investigated.

The static, dynamic and the total pressure distributions at the cross section of the considered pump are shown on Figure 11.10. Figure 11.10.a shows the distribution of the dynamic pressure. As expected, the maximum dynamic pressure occurs at the impeller outlet since the velocity reaches its maximum at this region. One of the duties of the diffuser is to convert this dynamic pressure to the static pressure. Figure 11.10.b shows the distribution of static pressure through the pump section. As seen from the figure, the static pressure is not high at the inlet surface, but it steadily increases up to the outlet of the pump. The variation of the total pressure through the pump is shown in Figure 11.10.c. Since static pressure is more dominant to the dynamic pressure, the behavior of the total pressure is similar to the static pressure. The distributions are also not symmetrical due to the rotation axis, because of the symmetrical structure of impeller and diffuser, and their position with respect to each others.

11.8. Pressure Distribution in the Impeller

In Figure 11.11, where the impeller is represented upside down without its shroud for a better view, the variation of static pressure contours on the blade and hub surfaces are shown for three different mass flow rates. The visual comparison of the static pressure distribution between figures shows that the static pressure decreases with the increasing flow rate as it is expected. This is what can be seen from the pump characteristic curve.

Figure 11.11.b shows distribution of static pressure on the impeller blade surfaces for the best efficiency point. This figure is very important for the designer, because the design of the pump is shaped for this point. The static pressure along the impeller blades and hub increases steadily through the impeller channel, and the isobars are formed perpendicular to the flow direction between the blades. The maximum static pressure is seen on the tip of the blade. Moreover, the minimum static pressure is observed at the suction side.

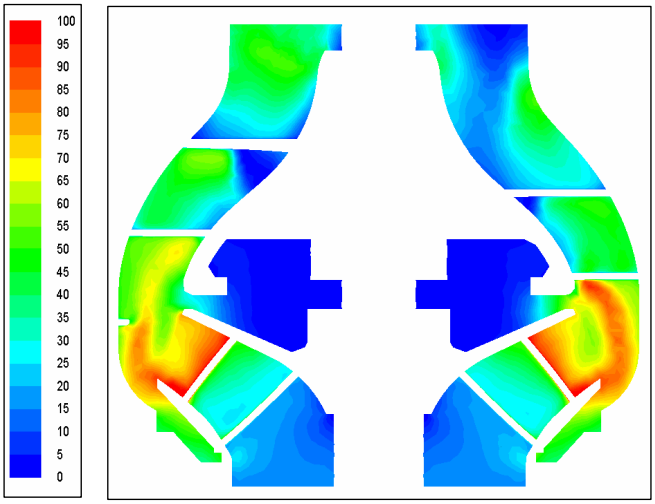

(a)

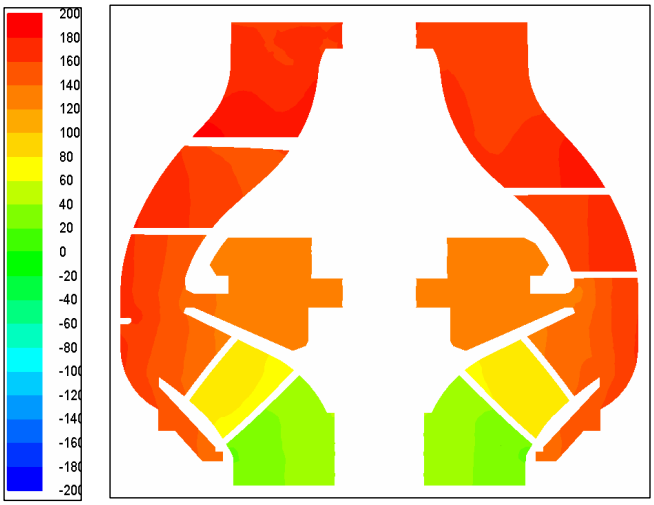

(b)

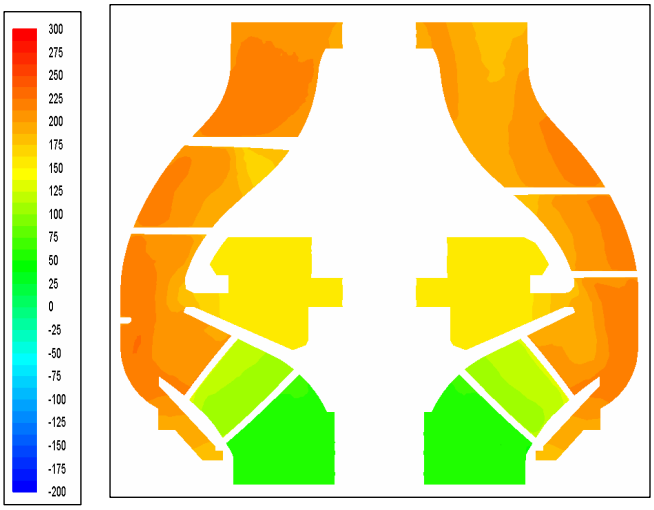

(c)

Figure 11.10. The dynamic (a), the static (b) and the total (c) pressure distribution over the pump cross section at its best efficiency point.

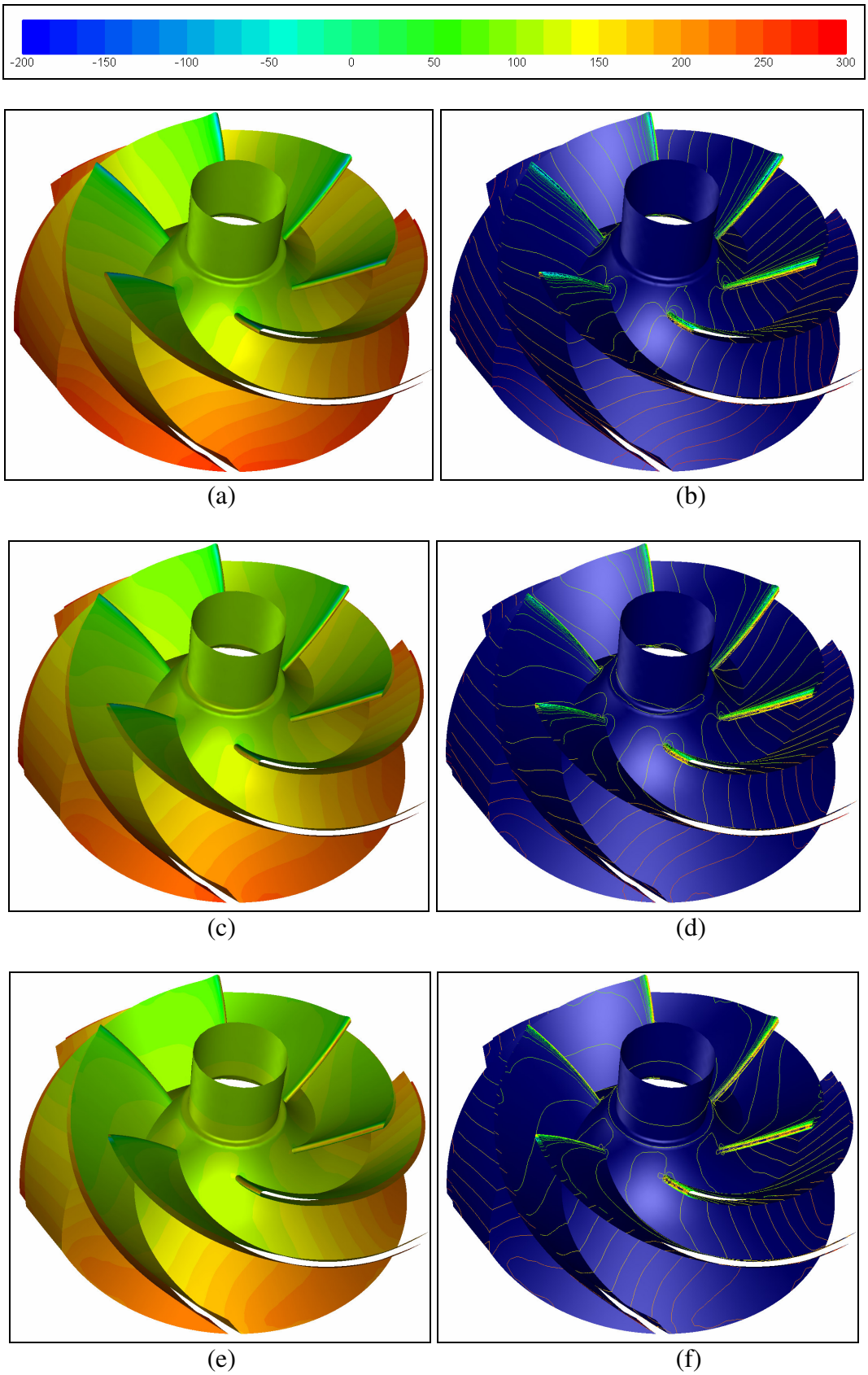

Figure 11.11. The static pressure distributions in the channel of the impeller for 90 kg/s (a-b), 120 kg/s (c-d), and for 150 kg/s (e-f) mass flow inlet.

In the Figure 11.11, the suction sides of the blades can be examined. Figure 11.12, where the hub and shroud surfaces are hided, shows variation of static pressure on the pressure side of the blades where the mechanical power is mainly converted to the hydrodynamic power. As seen, the static pressure is monotonically increases from the inlet of the impeller to the outlet. Like as the suction side, the pressure side of the vanes have also cascaded pressure increase through the impeller surface. The distortion at the outlet region, where the channel flow is ended, can also be observed. The distortion at the pressure for the outlet region of the impeller may be due to the effect of the diffuser blades.

11.9. Velocity Distribution Inside the Impeller

The relative velocity vectors on the hub and blade surfaces of the impeller are shown in Figure 11.13. Since the static pressure distribution is smooth, there is not any significant deviation from the path. The velocity increases smoothly. The angle of the vectors at the outlet region can also be calculated in order to control the design parameters.

The path lines of flow inside the impeller, which are colored by velocity magnitude, are shown in Figure 11.14. These path lines are released from the inlet surface of the impeller, follow the paths that are calculated at the design stage. As seen, they follow the channel between the blades without any distortions. The colors again indicate that magnitude of the velocity increases through the channel of the impeller.

The smooth increase in velocity magnitude, straight path lines that follow the blades, the velocity vectors perpendicular to the channel sections between the blades, and also the static and dynamic pressure distributions show that the design of the impeller achieves its duty and so the impeller design is successful.

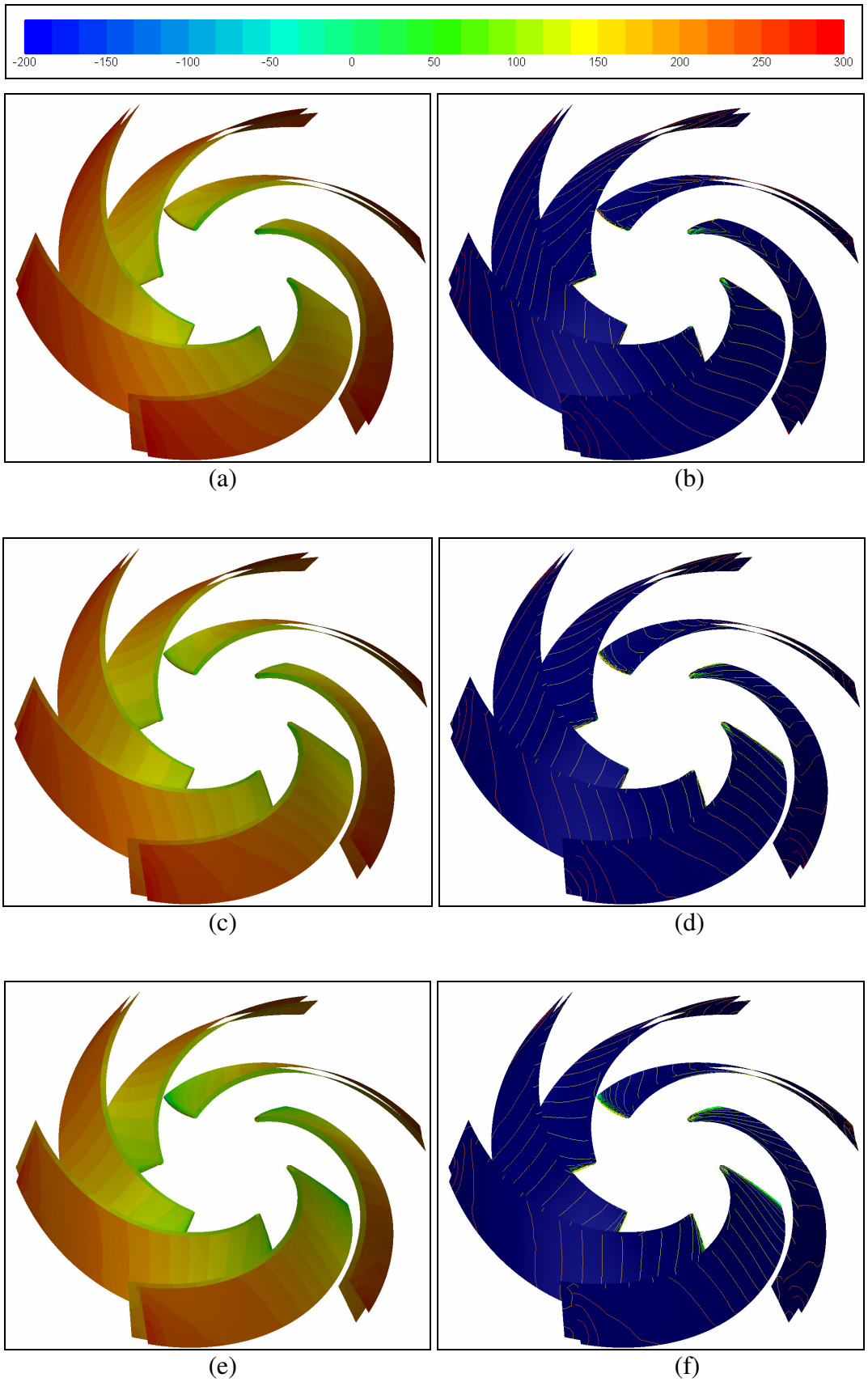

Figure 11.12. Distribution of static pressure on the active side of impeller for 90 kg/s (a-b), 120 kg/s (c-d), and for 150 kg/s (e-f) mass flow inlet.

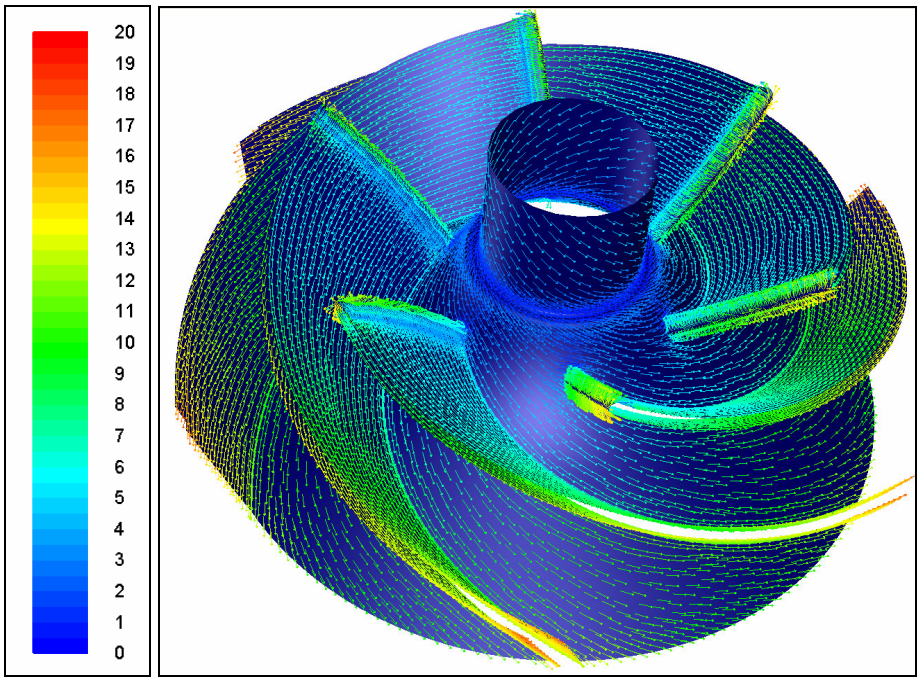

Figure 11.13. Relative velocity vectors through the impeller at 120 kg/s with 50 μm roughness.

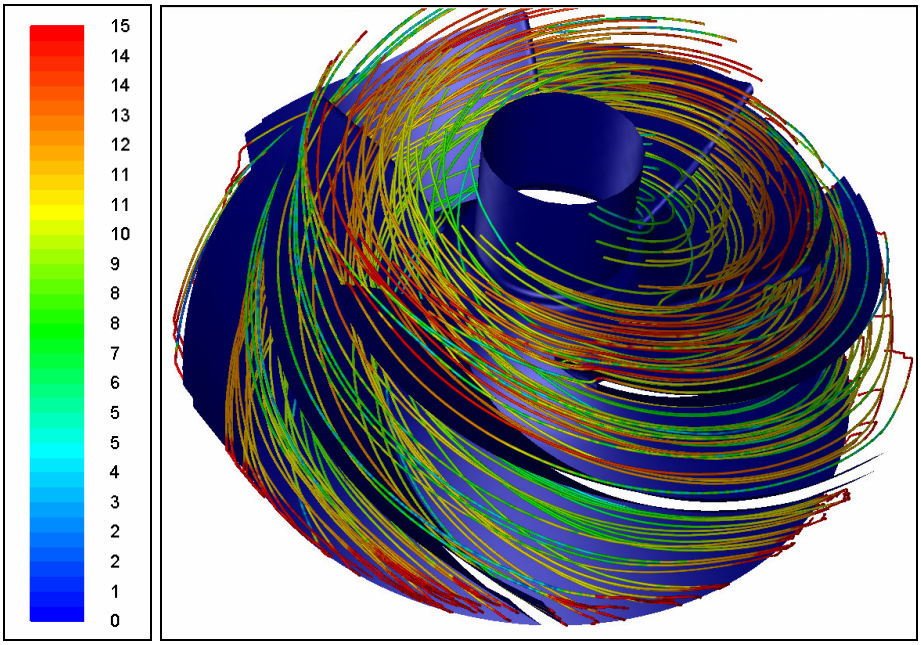

Figure 11.14. Path lines, that are colored by the relative velocity magnitude (m/s), released from the inlet of the impeller at 120 kg/s.

11.10. Pressure Distribution in the Diffuser

The diffuser part of the pump is also investigated. The static pressure distribution of the diffuser blades and the hub at three different flow rates are shown on Figure 11.6. As expected from the pump characteristic, the static pressure decreases as the flow rate increases.

The Figures 11.15.b and 11.15.c, where the pressure distribution for the best efficiency point at 50-micron roughness is represented, shows that there exists a disorder at the distribution near the discharge region. The pressure is not properly increasing through the path perpendicular to flow. Instead, it is increasing in the radial direction from hub to shroud. Since there is lower pressure on the hub surface, the fluid should flow from shroud surface to the hub surface. This causes turbulence, vortexes in the channel of the diffuser and thus the kinetic energy loss.

The path of the fluid in the channel between the diffuser blades and the velocity vectors through the diffuser blades should be investigated for a better comparison.

11.11. Velocity Distribution Inside the Diffuser

The diffuser velocity distribution, shown in Figure 11.16.a is not as good as the impeller velocity distribution. As mentioned in the previous section, since the pressure distribution changes on the blade surfaces is not perpendicular to the flow disturbances, turbulence and back flows occur inside the channel of the diffuser. As detailed in Figure 11.16.b, the backflows are mainly developed at the back of the stator impellers, where the pressure has the lowest value.

The Figures 11.17.a and b, which show the path lines released from the inlet of the diffuser and move forward through the channel. These figures prove what explained above. There are macro vortexes at the discharge of the flow because of the irregular pressure distribution. If the Figure 11.17.b is examined carefully, the path of the screws is found to be started from the shroud and directed into the hub surface, which also explained before. Another reason of the screws is the pressure difference between the side surfaces of the diffuser, at the outlet region. At this region, since the pressure at the front side is greater than the backside, the flow tends to direct to the lower pressure side, which also causes back flows and again kinetic energy loss at the discharge.

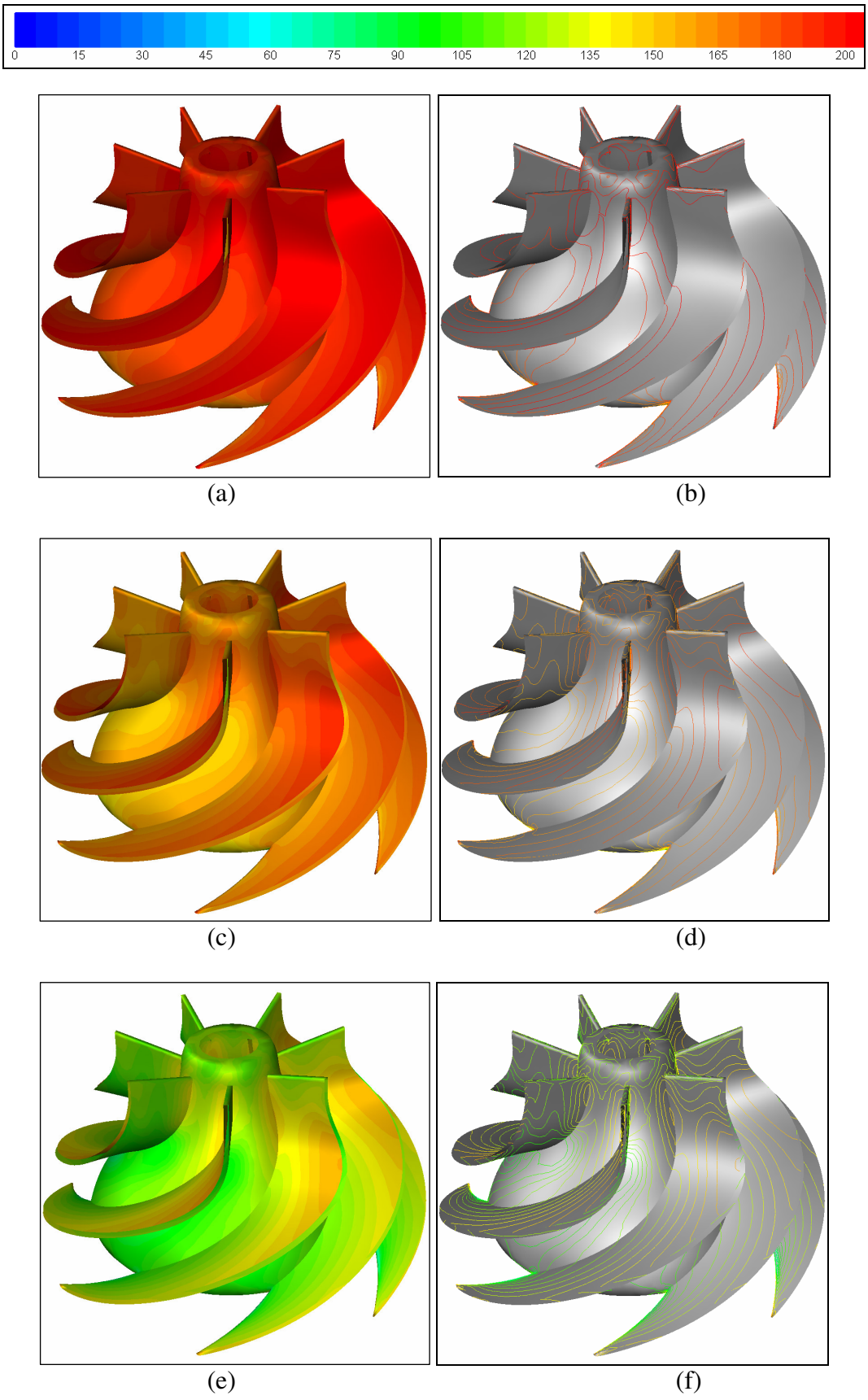

Figure 11.15. The static pressure distribution of diffuser (kPa) for (a) 90 kg/s, (b)120 kg/s and (c) 150 kg/s.

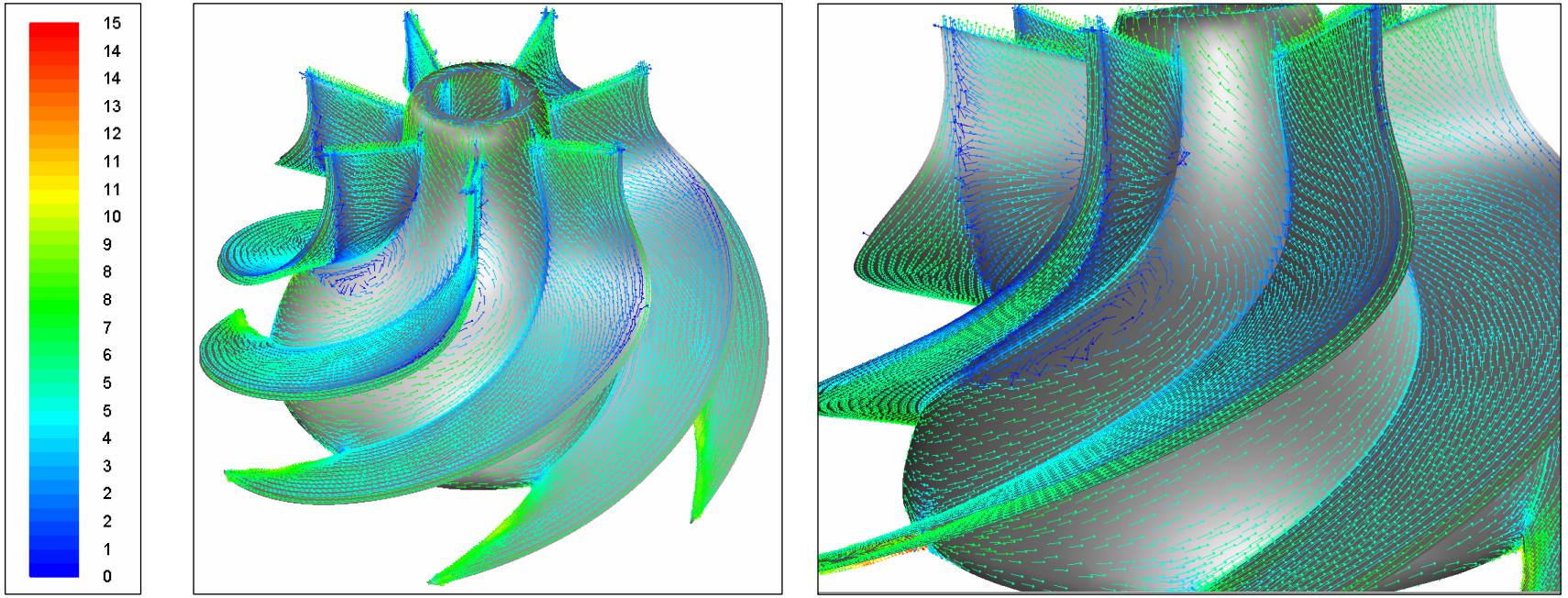

Figure 11.16. The velocity vectors inside the diffuser, colored by the velocity magnitude, at 120 kg/s flow rate.

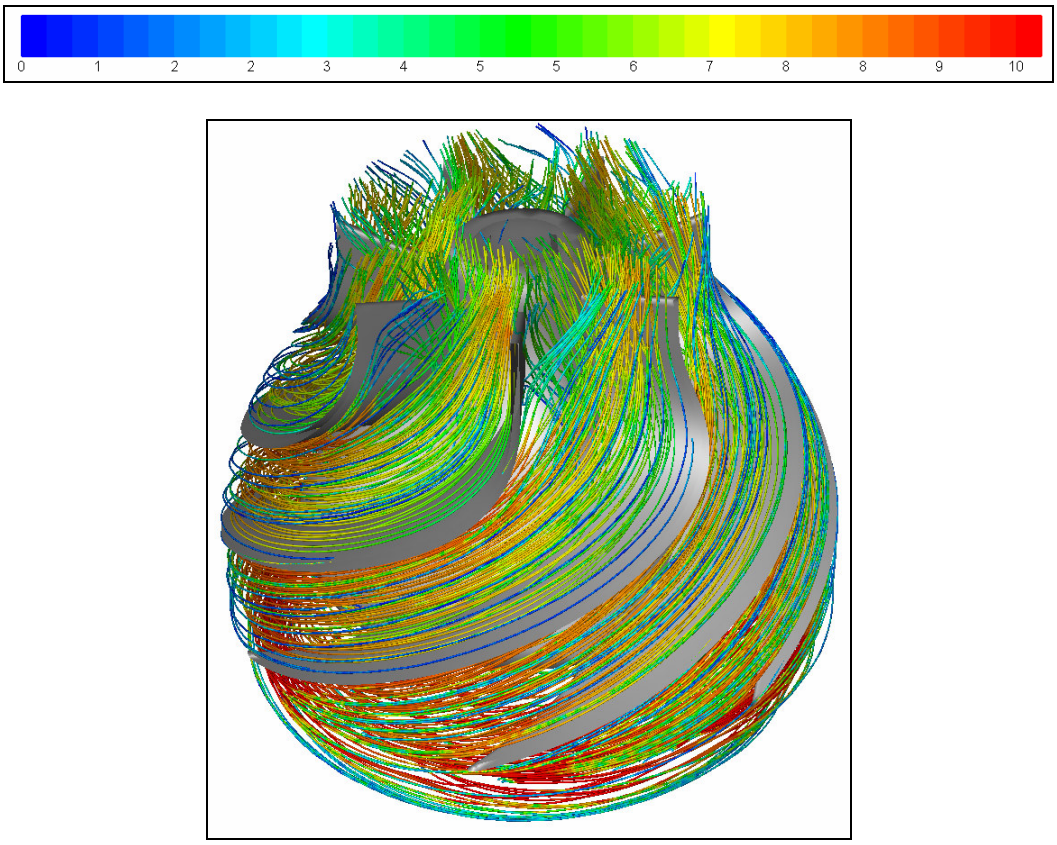

(a)

(b)

Figure 11.17. The path lines, released from the inlet of the diffuser, colored by the velocity magnitude (m/s) , at 120 kg/s flow rate.

CHAPTER 12

CONCLUSION

Pumps are machines that are providing transfer of fluids. From the various types of pump developed for different types of purposes, centrifugal pumps are the most efficient ones and are widely used in daily life. Deep well pumps constitute one of the subtypes of centrifugal pumps.

Since pumps are widely used, in response to the work done, they require high energy capacities. This brings the importance of the energy costs and thus the efficiency of the pump. The efficiency of the pump directly depends on the design of the pump. A proper design not only provides the operating conditions, but also provides the maximum possible efficiency. Therefore, searches are made in order to maximize the pump efficiency and to improve the pump design methods, which are mainly based on empirical methods. However, the designed pumps can not prove themselves until they are manufactured and tested in a calibrated test stand.

The traditional design and verification of the operating conditions is too expensive and takes long period. Computational fluid dynamics not only provides important information for designer, but also facilitates the test of the pump by the computers.

In the present study, a semi axial pump is investigated. A single stage pump belongs to Vansan Company is researched. The impeller and diffuser of the pump is modeled by AutoCAD and Unigraphics softwares. Then the mesh is generated by the Gambit program and data are transferred to the main program; Fluent.

The characteristic curve of the pump is obtained numerically and compared with the experimental curve of Duymuş. It is observed that there are differences between the numerical and experimental studies. In order to explain these differences, the pressure and the momentum were investigated individually.

The effect of roughness on the pump characteristic curves is also investigated. It is observed that by increasing the roughness, the head of the pump decreases, while the consumed power is almost constant. This causes the decrease of the efficiency at the same time.

The reason of the head loss is explained by the increase of the viscous forces. The increase of roughness increases turbulences in the boundary layer and consequently a part of the applied power is consumed to overcome the friction. Since the decrease in pressure moment compensates the increase of the viscous moment, the power seems to be almost constant.

The design of the impeller is proper. Fluid flows through the channel of the impeller and no vortexes or distortion forms in the channel. The isobars are perpendicular to the flow. No back flow is observed in the channel between the blades of the impeller.

On the other hand, there exist problems with the design of the diffuser. The increase of the pressure is not proper. The isobars are not perpendicular to the fluid flow. The pressure distribution causes forming of the vortexes in the channel of the diffusers. Thus, the design of the diffuser should be changed and a proper design should be replaced. The gain from the static pressure will increase, the friction losses decrease, the inlet of the second stage will be corrected, and the efficiency of the pump will increase.

The main difficulty of this study is the available computer sources. The computer technology is still not at the point for proper use of CFD codes. The analysis of just one point requires approximately 1000 iterations, which means the computers run for a night. The journal files, which enable to give commands computer during the analysis, make this analysis easier to be made.

Meshing the geometry is also a huge problem for the inexperienced users. The use of size functions, boundary layers and the interface regions is complicated and highly requires experience.

In order to improve this study, the following suggestions can be made:

- The pump, in actual working conditions has more than only a stage. A more proper geometry can be analyzed with discharge and suction case, even with two or more stages. Thus, the effect of the second impeller to the diffuser, the effect the flow straightening blades on the suction case and such interactions between the pump parts can be investigated.
- The effect of the other parameters like the turbulence models, pressure velocity coupling methods, different types of wall functions, pressure inlet condition, and even unsteady solution methods can be evaluated.

- During the experimental tests, the rotational speed and the efficiency of the motor are referred to its catalog data. However, instead of this, the rotational speed should be measured by the magnetic sensors, and the torque applied to the pump should be evaluated by a load cell. The change of rotational speed of the pump will affect the efficiency at third order of the change ratio.
- If the computational sources are available, the mesh can be developed. A mesh with more finite volumes will increase the resolution of the solution. Different mesh strategies, mesh structures like as hexahedral meshes can be employed instead of the tetrahedral meshes.
- The selected pump is a 14" pump. In order to see the effect of roughness in terms of viscous moment, a pump with a smaller geometry can be selected.

REFERENCES

Davidson, L., 2003, "*An Introduction to Turbulence Models*", Chalmers University Of Technology, (Chalmers, Göteborg, Sweden).

Değer, T., 2005, "Pompalarda Kavitasyon ve NPSH Karakteristiğinin Deney ve Sonlu Hacimler Yöntemi ile Incelenmesi", Ege University, Izmir.

Değer, T., Ertöz, A. Ö., Karamanoğlu, Y., 2004, "Pompa Test Standı Modernizasyonu", Turkish Pump and Valve Manufacturers Association 4th Congress, Istanbul.

Duymuş, E., 2003, "Değiştirilebilir Çarkli Pompalarda Teorik ve Deneysel Bir Araştirma.", Ege University, Izmir.

Edis, K., 1998, "*Hidrolik Makinalar Ders Notları*" I.T.Ü., Istanbul.

Ergün, E. S., 1999, "Numerical Modelling and Analisis of Centrifugal Pumps", Boğaziçi University, Istanbul.

Ferziger, J. H., Peric, M., 2002, "*Computational Methods for Fluid Dynamics – 3rd Edition*", (Springer – Verlag, Berlin, Germany).

Fluent Inc., 2005, "*Fluent 6.2 User's Manual*", Centerra Resource Park 10 Cavendish Court, Lebanon.

Frenning, L., Hovstadius, G., Alfredsson, K., Beekman, B., Angle, T., Bower, J., Hennecke, F., McKane, A., Doolin, J., Romanyshyn, G., 2001, "*Pompalarda Ömür Boyu Maliyet: Pompali Tesisler Için Ömürboyu Maliyet Analiz Rehberi*", Translated by Konuralp, O, Hydraulic Institute and Europump, Brussels, Belgium, Turkish Pump and Valve Manufacturers Association, Publication No:12.

Karakaş, A.A., 2000, "Radyal Pompa Çarkları İçerisindeki Üç Boyutlu Sürtmeli ve Sürtmesiz Akışın Sayısal Analizi", I.T.U., Istanbul.

Karamanoğlu, Y., Mobedi, M., Ertöz. A. Ö., 2005, "Pompa Tasarimi Geliştirilmesinde Hesaplamali Akişkanlar Dinamiğinin Kullanilmasi", Turkish Chamber of Mechanical Engineers 7th National Congress, (23-26 November 2005), Izmir, p 351.

Karassik, I. J., Krutzsch, W. C., Fraser, W. H., Messina, J. P., 1986, "*Pump Handbook Second Edition*", (McGraw – Hill, Malaysia).

Lomax, H., Pulliam, T. H., Zingg, W. D., 1999, "*Fundemantals of Computational Fluid Dynamics*", Nasa Ames Research Center.

Pınarbaşı, A., 2003, "*Akışkanlar Mekaniği Ders Notları*", Cumhuriyet University, Mechanical Engineering Department, Sivas.

Sarıoğlu. K., 1997, "Pompa Çarkları Içindeki Akışın Sayısal Çözümlenmesi", I.T.U, Istanbul.

Sarıoğlu, K., Ayder, E., 1997, "Numerical Calculation of the Flow Inside Pump Impellers Using 3D Euler Equations", I.T.U. Istanbul.

Stepanoff, A., 1957, "*Centrifugal and Axial Flow Pumps, Theory, Design and Application*", John Wiley and Sons Inc., 2nd Edition.

van Esch, B.P.M., 1997, "Simulation of Three Dimensional Unsteady Flow in Hydraulic Pumps", University of Twente, Netherlands.

Vansan Company Product Catalogues and Technical Documents, 2000-2003, Vansan Company, 10035 sok No:10 A.O.S.B Çiğli İZMİR.

Versteeg, H. K., Malalasekera, W., 1995, "*An Introduction to Computational Fluid Dynamics – The Finite Volume Method*", (Longman, London).